Heliyon 6 (2020) e05388

Contents lists available at ScienceDirect

Heliyon

journal homepage: www.cell.com/heliyon

Research article

The relationship between properties of plant-based biochars and sorption of Cd(II), Pb(II) and Zn(II) in soil model systems

Rosa I. Soria [a,*], Stephen A. Rolfe [b], Mauro Pazmiño Betancourth [c], Steven F. Thornton [a]

[a] Civil and Structural Engineering Department, Sheffield University, Sheffield, S102TN, United Kingdom
[b] Department of Animal and Plant Science, Sheffield University, Sheffield, S102TN, United Kingdom
[c] School of Engineering, University of Glasgow, Glasgow, G12 8QQ, United Kingdom

ARTICLE INFO

Keywords:
Environmental chemistry
Environmental management
Environmental pollution
Soil chemistry
Soil pollution
Soil pore water
Cooperative sorption
S-shape isotherm
Hill-isotherm
Correlation analysis
Trace elements

ABSTRACT

Plant based biochars are proposed as soil amendments to immobilize potentially toxic trace elements (PTEs), such as Cd(II), Pb(II) and Zn(II) and aid in soil restoration. However, the sorption capacity of biochar for these elements can vary widely depending on biochar nature and metal properties. Currently, there is no clear methodology to pre-screen biochars for their suitability as adsorbents for these elements. Therefore, to facilitate biochar selection for application in soil restoration, this study explored the relationships between the physico-chemical properties of five plant-based biochars and their capacity to immobilize Cd(II), Pb(II) and Zn(II). Batch experiments using synthetic soil pore water were used to assess the sorption of these elements. The sorption isotherms described by the Hill model indicated that PTE sorption capacity followed the order Pb(II) > Cd(II) >Zn(II) regardless of biochar type in mono-element systems. Preferential sorption of Pb(II) limited the immobilization of Cd(II) and Zn(II) in multi-element systems. ATR-FTIR and SEM-EDX spectroscopy studies indicated that Cd(II) and Pb(II) sorption was mediated by complexation with carboxylic groups, cation–π interactions and precipitation with phosphates and silicates, while Zn(II) sorption occurred mainly by complexation with phenolic groups and precipitation with phosphates. A high correlation (>0.8) between Electrical Conductivity, Cation Exchange Capacity, pH and sorption capacity was identified for all metals tested, highlighting the electrostatic nature of the sorption mechanisms involved. Biochars derived from herbaceous feedstock were better candidates for remediation of soil polluted with Cd(II), Pb(II) and Zn(II), rather than wood-derived biochar. Overall, this study provides evidence of the direct relationship between specific properties of plant-based biochars (pH and EC) and their suitability as adsorbents for some PTEs in soil systems.

1. Introduction

Potentially toxic trace elements (PTEs) are important environmental pollutants due to their widespread occurrence. The use of the term PTEs has gained favour as it is more inclusive and appropriate than "heavy metals" (Shaheen et al., 2013). Currently, most PTEs enter the environment from industrial and mining activities (Su et al., 2014). In terrestrial systems, soil is the major repository of trace elements (Wang et al., 2018). Elevated concentrations of PTEs in soils can result in non-desirable effects such as a reduced agricultural productivity, phytotoxicity and bioaccumulation (Bandara et al., 2017).

Cost-effective management solutions are required to reduce the environmental risk from PTE-contaminated soil. Of the PTEs commonly present in polluted soils, Pb(II), Cd(II) and Zn(II) are most problematic, according to reported potential toxicity at the lowest bioavailable concentration (Di Bonito, 2005; Sparks, 2003). Recent studies highlight biochars as effective amendments for improving soil health at contaminated sites. This is achieved by reducing bioavailable concentrations of PTEs (Wang et al., 2019; Yang et al., 2017). Among different feedstock types, biochars derived from plant waste are gaining attention as a means to recycle agricultural wastes (Domingues et al., 2017).

Biochar is a black carbon obtained by thermal degradation processes, through which residual biomass is converted into a charred material at temperatures between 300 °C and 700 °C (Lehmann et al., 2011; Mandal et al., 2017). Biochar is rich in functional groups (e.g. carboxylic, hydroxyl, and amino groups), with a high micro- and meso-porosity, large surface area, high pH and cation exchange capacity (CEC); therefore, it may be a surface adsorbent for PTE

* Corresponding author.
E-mail address: risoriapenafiel1@sheffield.ac.uk (R.I. Soria).

https://doi.org/10.1016/j.heliyon.2020.e05388
Received 21 July 2020; Received in revised form 5 October 2020; Accepted 27 October 2020

immobilization (Caporale et al., 2014; Wang et al., 2018). The metal sorption process by biochars has been previously described as a result of three different mechanisms: (i) ion exchange (Ca^{2+},K^{+},Mg^{2+},Na^{+}); (ii) metal complexation onto free and complexed carbonyl, carboxyl, alcoholic, hydroxyl or phenolic hydroxyl functional groups; and (iii) physical adsorption or surface precipitation caused by sorptive interaction involving delocalization of π electrons of organic carbon (Trakal et al., 2014). It is known that pyrolysis conditions and feedstock origin are key factors determining biochar properties and consequently its sorption capacity (Janus et al., 2015). However, adsorption of PTEs is also influenced by element properties and their competitive behaviour for biochar sorption sites (Park et al., 2016). Because biochar is not a well-defined material, the identification of biochars with beneficial properties for soils is complicated, resulting in large variation in sorption potential and performance (Keiluweit et al., 2010). In the case of PTE immobilization in soil, it is not yet clear what determines the binding affinity and interactions between biochar and PTEs in the complex soil environment (Wang et al., 2019).

Sorption of PTEs by biochar is usually determined with batch studies. However, most sorption studies have focused on water treatment, using high PTE concentrations up to 1000 $mg.L^{-1}$ (Ma et al., 2016; Wang et al., 2015; Xiang et al., 2020) which are much greater than bioavailable concentrations of PTEs in soil. Soils with very large PTE concentrations commonly have a small bioavailable fraction due to the presence of insoluble mineral phases (Giller et al., 1998). The bioavailable PTE concentrations reported in soil pore water from contaminated soils vary between 0.1 to 4 $mg.L^{-1}$ for Cd and Zn, but 0.1–90 $mg.L^{-1}$ for Pb (Moreno et al., 2011; Schweiker et al., 2014).

We hypothesised that biochar sorption capacity for Cd(II), Pb(II) and Zn(II) is determined by a limited number of biochar properties. Understanding which are the key properties of plant-derived biochars controlling the sorption for these elements can serve as a basis to assess and select suitable biochars for the remediation of PTE-contaminated soil. The aim of this study is to establish relationships between the physicochemical properties of five plant-based biochars and the immobilization capacity for Cd(II), Pb(II) and Zn(II) in synthetic soil pore water. This will allow biochar properties to be identified that can be used to build predictive models of biochar sorption potential.

2. Materials and methods

2.1. Biochar description

Five biochars produced from different plant-derived feedstocks were obtained from the UK Biochar Research Centre. These were converted under well-controlled and reproducible process conditions, comprising a rotary kiln pyrolyser heated indirectly and electrically (Mašek et al., 2018). The feedstock included oil seed rape straw (OSR550, OSR700), wheat straw (WSP550), Miscanthus straw (MSP550) and soft wood (SWP550) pellets. Selected biochar properties provided by the supplier are shown in Table 1, with other properties determined in this study experimentally. The material used in the study was the fraction passing through a 2 mm stainless steel sieve screen after grinding manually with a mortar and pestle.

2.2. Biochar characterization

The cation exchange capacity (CEC) of biochar was determined using the silver thiourea (AgTU) method, as described by Jiang et al. (2017) and the porosity was studied using the N_2 adsorption method at 77 K with an ASAP 2010 porosity analyser (Micrometrics, USA). Pore size distribution was determined by the Barrett–Joyner–Halenda (BJH) analysis, and biochar surface area was determined using the Brunauer-Emmett-Teller (BET) method; measurements were based on 15 analysis points using the 3 Flex 4.04 software. Samples were degassed overnight (16 h) at 100 °C in a Vacprep 061 prior to analysis (Micrometrics Sample Degas System, USA).

2.3. Adsorption experiments

A synthetic soil pore water solution resembling the average ion composition of UK soil solution (Kinniburgh and Miles, 1983) was used for the sorption tests. Only major anions and cations were considered in the make-up of the synthetic soil pore water by dissolving the following salts in deionized water: KNO_3 (49.52 $mg.L^{-1}$), $NaNO_3$ (26.33 $mg.L^{-1}$), $Mg(NO_3)_2.6H_2O$ (31.089 $mg.L^{-1}$), $CaCl_2.2H_2O$ (55.19 $mg.L^{-1}$), $CaSO_4$ (43.55 $mg.L^{-1}$), $Ca(NO_3)_2.4H_2O$ (181.71 $mg.L^{-1}$). The ionic strength of this solution was 5 mM, with a pH of 6.8.

Table 1. Biochar properties.

Source	Oil seed rape straw pellets		Wheat straw pellets	Miscanthus straw pellets	Soft wood pellets
Biochar notation	OSR550	OSR700	WSP550	MSP550	SWP550
Temperature (°C)[1]	550	700	550	550	550
pH	9.8 ± 0.5	10.4 ± 0.5	9.9 ± 0.2	9.8 ± 0.2	7.9 ± 0.3
$H:C_{tot}$ (molar ratio)[1]	0.32 ± 0.03	0.19 ± 0.02	0.4 ± 0.1	0.38 ± 0.04	0.39 ± 0.01
$O:C_{tot}$ (molar ratio) [1]	0.12 ± 0.02	0.09 ± 0.02	0.1 ± 0.0	0.09 ± 0.03	0.09 ± 0.01
Ash content [wt%]*[1]	19 ± 2	21.9 ± 0.5	21 ± 1	12 ± 1	1.3 ± 0.4
Electric conductivity [$dS.m^{-1}$] [1]	2.3 ± 0.4	3.1 ± 0.4	1.7 ± 0.4	0.8 ± 0.2	0.09 ± 0.03
Total N [wt%]*[1]	1.6 ± 0.2	1.3 ± 0.2	1.4 ± 0.1	0.8 ± 0.1	<0.10
Total P [wt%]*[1]	0.29 ± 0.08	0.3 ± 0.1	0.14 ± 0.02	0.19 ± 0.04	0.06 ± 0.04
Total K [wt%]*[1]	2.9 ± 0.3	2.9 ± 0.4	1.6 ± 0.4	0.9 ± 0.1	0.3 ± 0.1
Total pore volume [$cm^3.g^{-1}$][2]	0.38 ± 0.02 c	0.42 ± 0.01 b	0.27 ± 0.01 e	0.6108 ± 0.0003 a	0.33 ± 0.01 d
BET [$m^2.g^{-1}$][2]	416 ± 5 c	461 ± 5 b	299 ± 3 e	490 ± 12 a	358 ± 3 d
CEC [$cmol.kg^{-1}$][2]	22 ± 3 a	23 ± 1 a	21 ± 2 a	22 ± 1 a	11 ± 3 b

BET: specific surface area determined by the Brunauer-Emmett-Teller (BET) method.
CEC: cation exchange capacity.
* Dry basis.
[1] Data reproduced from UK Biochar Research Centre, values are means ± run to run variation (SD), (http://www.biochar.ac.uk/standard_materials.php; Accessed 17/08/2020).
[2] Data determined experimentally in the present study, values are means ± standard deviation; n = 3; different letters indicate significant differences between biochars ($p < 0.05$; one-way ANOVA, Tukey's honestly significant difference (HSD) post hoc test).

The metal adsorption experiments were performed using a batch equilibration technique in triplicate. Stock solutions (1000 mg.L^{-1}) of Zn(II), Cd(II), and Pb(II) were prepared in deionized water from $Zn(NO_3)_2.6H_2O$, $Cd(NO_3)_2.4H_2O$ and $Pb(NO_3)_2$ (GR grade, Fisher Scientific, USA).

2.3.1. Kinetics

The effect of contact time on the adsorption capacity of biochars for Cd(II), Pb(II) and Zn(II) as single element solutions was studied. The kinetic experiments were conducted in 50 mL polyethylene centrifuge tubes containing 100.0 ± 0.3 mg of biochar and 20 mL of 5000 µg.L^{-1} soil solution of each element, preadjusted to pH 7 (average pH of pore water in UK soils) using 0.1 M NaOH solution. The mixture was agitated at 120 rpm on a reciprocating shaker at 22 ± 2 °C. Replicate tubes for each biochar were destructively sampled at 10 time points (0, 1, 2, 4, 8, 12, 24, 48, 72 and 96 h), and filtered using 0.45 µm syringe filters. The filtrates were acidified with 1% (v/v) HNO_3 (Fisher, TraceMetal™ grade) and the concentration of Cd(II), Pb(II) and Zn(II) determined by ICP-MS (PerkinElmer, Sciex Elan DRCII).

2.3.2. Effect of pH on adsorption tests

The impact of soil pore water pH on PTE sorption capacity was determined as described above except that the initial pH of the solutions was adjusted to values between 4.0 and 9.0 ± 0.3 using 0.1 M NaOH or 0.1 M HCl. This is the pH range commonly present in UK soil solutions (Kinniburgh and Miles, 1983). The chemical speciation of Cd(II), Pb(II) and Zn(II) at different initial pH values was studied using visual MINTEQ 3.1 (https://vminteq.lwr.kth.se/).

2.3.3. PTEs sorption capacity

Sorption capacity for the PTEs was measured using a constant quantity (1.25 mg.L^{-1}) of biochar. Trace element solutions were prepared in the range commonly present in the soil pore water of contaminated soils: from 0.05 to 10 mg.L^{-1} for Cd(II) and Zn(II) and from 0.5 to 50 mg.L^{-1} for Pb(II). As the biochar did not reach its maximum sorption capacity within that range additional concentrations up to 50 mg.L^{-1} were used for Cd(II) and Zn(II) and up to 85 mg.L^{-1} for Pb(II). Sorption experiments were carried out at an initial pH 5 for Pb(II) sorption, pH 6.5 for Cd(II) and pH 7.5 for Zn(II). After filtration, biochar samples loaded with Cd(II), Pb(II) and Zn(II) were recovered and rinsed with deionized water, then dried at 22 °C ± 2 °C. Attenuated Total Reflection Fourier Transform Infrared (ATR-FTIR) spectra of loaded biochars were obtained using a dry-air purged Bruker Vertex 70 spectrometer equipped with a KBr splitter, a DLaTGS detector and a diamond crystal accessory (Bruker Platinum ATR Unit A225). The spectra were acquired between 400 and 2000 cm^{-1} with a resolution of 1 cm^{-1} and are an average from 16 scans. Spectra were acquired in random order, in duplicate. The ATR-FTIR spectra was normalized with Orange 3.25 (Demsar et al., 2013). The normalized spectra was used to conduct a principal component analysis (PCA) in R (R Core Team, 2013). Since it is possible that ATR-FTIR spectra might contain small differences between biochars that could not be distinguished visually, multivariate data tools as PCA are necessary for spectra analysis. PCA is an effective variable reduction technique for spectroscopic data (Lazzari et al., 2018). Scanning electron microscopy coupled with Energy Dispersive X-Ray Spectroscopy (SEM-EDX) was conducted on PTE-loaded biochars using an Inspect F50 (FEI, US) and AZtec (Oxford Instruments) respectively; 20 kV with spot size 4 were used and point ID area analysis and electronic x-ray mapping were assessed in raw and PTE-loaded samples.

2.3.4. Competitive sorption

Competitive sorption effects were evaluated in binary and ternary systems of the studied PTEs. Initial concentrations that induced an intermediate sorption capacity by biochars in the single sorption test were used in this competitive experiment; the initial concentrations were: Zn(II) 13 mg.L^{-1}, Pb(II) 41 mg.L^{-1} and Cd(II) 22 mg.L^{-1}, which are equivalent to 0.2 mM in each case. Equimolar concentrations were used in this test to allow comparison between elements; the combinations were: Zn(II):Cd(II), Pb(II):Cd(II), Zn(II):Pb(II) and Cd(II):Zn(II):Pb(II). The pH was 6.5 for the first combination and 5 for the rest, as required for the evaluation of Pb binding. Pb(II) is present as insoluble $Pb(OH)_2$ at pH 5.5–12.5 (Li et al., 2017), which would limit the amount of soluble Pb^{2+} that can bind with biochar.

2.4. Sorption models

2.4.1. Kinetic models

First-order (Lagergren, 1898) and second-order (Ho and McKay, 1998) kinetic models presented in Eqs. (1) and (2) respectively were fitted to the experimental data to elucidate the sorption rate and kinetic parameters, instead of the linearized versions.

$$Q_t = Q_e\left(1 - e^{-k_1 t}\right) \tag{1}$$

$$Q_t = \frac{k_2 Q_e^2 t}{1 + k_2 Q_e t} \tag{2}$$

where Q_t and Q_e (mg.g^{-1}) are adsorbed Cd(II), Pb(II) and Zn(II) at any time and at equilibrium, t is the time (min) and k_1 (min^{-1}) and k_2 (g.mg^{-1}.min^{-1}) are the rate constants. The amount of immobilized trace elements onto biochars, Q_t (mg.g^{-1}), was calculated as described in Eq. (3)

$$Q_t = \frac{(C_0 - C_t)\,V}{m} \tag{3}$$

where C_0 and C_t (mg.L^{-1}) are Cd(II), Pb(II) or Zn(II) concentrations at time zero and time t respectively, V (L) is the volume of synthetic soil pore water solution and m (g) is the weight of biochar used in each tube. At equilibrium Q_t and C_t are referred as Q_e and C_e respectively (Cui et al., 2016b). To select the best statistical model we used a penalized likelihood criterion known as Akaike Information Criterion (AIC) developed by Akaike (1974). AIC penalizes the number of parameters of a model and allows the goodness of fit of a model to be balanced against its degrees of freedom. The model for which AIC is minimal is selected as the one that best describes the experimental data (Akpa and Unuabonah, 2011). The general form for calculating the AIC is given in:

$$AIC = -2log(L) + 2n_{par} \tag{4}$$

where, L is the likelihood of the fitted model and n_{par} is the total number of parameters in the model. AIC has been reported as a better criterion for ranking sorption models instead of the error functions (sum of absolute error, average relative error, sum of square error, coefficient of determination, chi-squares, etc) due to its high sensitivity to model deviations (Akpa and Unuabonah, 2011). The AIC values for the fitted models were estimated using the AIC function from R (R Core Team, 2013).

2.4.2. Adsorption isotherm models

To evaluate the sorption of Cd(II), Pb(II) and Zn(II) by the studied biochars, the commonly used Langmuir (1918), Freundlich (1906), and Temkin (Temkin and Pyzhev, 1940) sorption models presented in Eqs. (5), (6), and (7) were examined. Additionally, models that adapt to describe S-shape isotherms, such as Dubinin-Radushkevich (Dubinin, 1975) and Hill model (Hill, 1910) presented in Eqs. (8) and (9), were studied.

$$Q_e = \frac{K_l q_m Ce}{1 + K_l Ce} \tag{5}$$

Where, q_m (mg.g^{-1}) is the maximum adsorption capacity of biochar for Cd(II), Pb(II) or Zn(II) and K_l (L.mg^{-1}) is the Langmuir constant related to the affinity of the binding sites (Cui et al., 2016b).

$$Q_e = K_F C e^{\frac{1}{nF}} \quad (6)$$

Where, K_F (mg·g^{-1}) is the Freundlich constant and nF is the Freundlich exponent related to adsorption intensity (Cui et al., 2016b).

$$Q_e = \left(\frac{RT}{b}\right) lnA + \left(\frac{RT}{b}\right) Ce \quad (7)$$

Where, A (g^{-1}) is the Temkin constant, b (J.mol^{-1}) is the constant related with the heat of sorption, R is the gas constant (8.31 J.mol^{-1}·K^{-1}) and T (K) is the absolute temperature.

$$Q_e = q_m \exp\left\{ -\beta \left[RT\ ln\left(\frac{Cs}{Ce}\right)\right]^2 \right\} \quad (8)$$

Where, β (mol^2 kJ^{-2}) is the Dubinin-Radushkevich constant related to the adsorption energy and Cs (mg.L^{-1}) is the solubility of the solute (Hu and Zhang, 2019).

$$Q_e = q_m \frac{C_e^n}{K_H + C_e^n} \quad (9)$$

Where, K_H (mg.L^{-1}) is the Hill constant that represents the concentration for which Q_e is equal to 0.5 q_m (hence an expression of affinity and/or sensitivity of the system) (Goutelle et al., 2008) and n (dimensionless) is the Hill coefficient of sigmoidicity which is related to the degree of cooperation between binding sites (Martucci et al., 2015).

Biochar SWP550 was excluded from the model fitting as it showed little PTE sorption (data not shown), possibly due to a low CEC. Instead the maximum sorption capacity determined experimentally was used for comparison.

2.5. Statistical analysis

The data was analysed using R (R Core Team, 2013). Differences in BET, CEC and pore volume were analysed using linear regression followed by ONE WAY ANOVA. Differences in sorption capacities due to the contact time (kinetic study) and pH, were analysed by using linear regression followed by TWO WAY ANOVA. Tukey's honestly significant difference (HSD) post hoc test was used to determine significant differences among groups in the before mentioned analysis.

In order to determine statistical differences in the parameters obtained from nonlinear model fitting (kinetics and Hill isotherm), data were subset by element. Two non-linear regressions for each of the respective equations (second order kinetic model and Hill equation) were performed using biochar type as the grouping variable; the first non-linear regression allowed the fitted model parameters to be different for each biochar (model 1) while in the second non-linear regression the parameters were set to be the same for all biochars (model 2), as recommended by (Ritz and Streibig, 2009). Thereafter a ONE WAY ANOVA comparing model 1 against model 2 was conducted as a pairwise comparison between biochars for each of the fitted parameters to establish significant differences between biochars. The raw data and the coding (R script) for fitting the Hill and Langmuir adsorption isotherm models as well as the code to analyse statistical differences in the parameters derived from the Hill model between biochars can be accessed at Soria et al. (2020).

2.5.1. Correlation analysis

A Pearson correlation analysis was conducted to understand the relationship between biochar maximum sorption capacities (q_m) for Cd(II), Pb(II) and Zn(II) and biochar physical and chemical properties. The q_m (mg.g^{-1}) values were derived from the Hill isotherm; however in the case of SWP550 the highest experimentally-determined sorption capacity was used. The biochar properties used in the analysis were CEC [cmol.kg^{-1}], BET [m^2.g^{-1}], total pore volume [cm^3.g^{-1}], total K [wt%], total P [wt%], total N [wt%], EC [dS.m^{-1}], O:C$_{tot}$ (molar ratio), H:C$_{tot}$ (molar ratio) and pH (Table 1). Also, the functional groups Si–O, C–H, C–O, COH and COOH from the ATR-FTIR analysis were included using the absorbance values from normalized spectra of raw biochars. The correlation was conducted at 95% confidence using R (R Core Team, 2013) and the results were presented as a heat map.

2.5.2. Linear models to describe biochar sorption capacity

Linear regression analysis was conducted to determine if biochar sorption capacity for Cd(II), Pb(II) and Zn(II) can be described as a function of its physico-chemical properties. The regression considered the same biochar physico-chemical properties used in the correlation analysis (section 2.5.1) as single predictor variables and when there was poor linearity ($r^2 < 0.8$), a second variable was introduced. The maximum sorption capacities (q_m) of the biochars for Cd(II), Pb(II) and Zn(II) estimated with the Hill model were used as the response variable. The AIC criterion determined the parameters that produce the most suitable model describing the sorption capacity for each element.

3. Results and discussion

3.1. Biochar characterization

The physico-chemical properties of the biochars are presented in Table 1. The BET surface area varied depending on the feedstock used, the highest was MSP550 (490 m^2.g^{-1}) and the lowest was WSP550 (299 m^2.g^{-1}). These BET areas were correlated with the total pore volume, in the order: MSP550 > OSR700 > OSR550 > SWP550 > WSP550.

Biochars produced from herbaceous biomass (WSP550, MWSP550 and OSRs) had a significantly higher CEC ($p < 0.001$), from 20.65 to 23.29 cmol.kg^{-1}, than biochar SWP550 produced from the wood feedstock, with a CEC of 11.23 cmol.kg^{-1}. The CEC of SWP550 was similar to that of a biochar obtained from pinewood produced at 650 °C (from 7.0 to 11.9 cmol.kg^{-1} at different pH) reported by Mukherjee et al. (2011). Similarly, Domingues et al. (2017) reported lower CEC values (2.4–10.8 cmol.kg^{-1}) for three wood-derived biochars relative to coffee husk biochar (69–72 cmol.kg^{-1}) and chicken manure biochar (23 cmol.kg^{-1}).

3.2. PTEs sorption experiments

3.2.1. Kinetics

The effect of contact time on Zn(II), Cd(II) and Pb(II) sorption by the biochars is presented in Figure 1A. PTE adsorption was fast during the first 4 h (90–95 % of trace elements sorption) and complete by 24 h. Therefore, 24 h was selected as the equilibrium time.

Calculation of AIC coefficients (Table 2) indicated that the second order kinetic model best described the data. At equilibrium the value of k_2 indicated that sorption occurred in the following rate order: Pb(II) >Zn(II) >Cd(II) for biochars MSP550 and WSP550, Zn(II) >Pb(II) >Cd(II) for biochars OSR550 and OSR700, and Cd(II) >Pb(II) >Zn(II) for biochar SWP550. The sorption capacity (Q_e) for Pb(II) was lower than that for Cd(II) and Zn(II) for all the biochars except SWP550, whose performance was significantly lower ($p < 0.05$) than the rest of biochars for all metals tested (Table 3). The lower sorption capacity for Pb(II) is attributed to the initial pH of the solution (pH 7). In natural systems Pb(II) is present mainly as soluble species Pb^{2+} and $Pb(OH)^+$ at pH < 5.5, but as insoluble forms, $Pb(OH)_2$, at pH 5.5–12.5 and $Pb(OH_4)^{2-}$ at pH > 12.5 (Li et al., 2017). This is consistent with other biochar sorption studies which describe the formation of Pb(II) metal hydroxide precipitates at pH > 5 (Naidu et al., 2013; Yang et al., 2016). The formation of Pb(II) precipitates reduces the amount of soluble Pb(II) forms that can interact with biochar surface binding sites. Therefore, in soil pore water with pH > 5, Pb(II) immobilization by biochar will be restricted by the amount of Pb(II) soluble species.

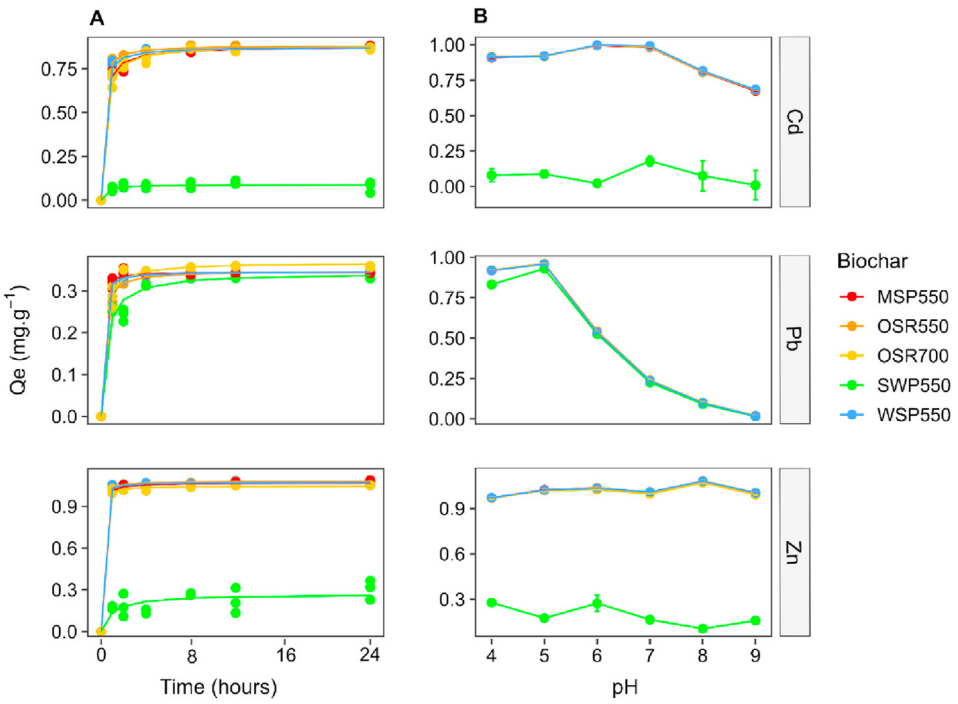

Figure 1. Effect of contact time and solution pH on sorption capacity of Cd(II), Pb(II) and Zn(II). A) Sorption kinetics during the first 24 h using a background solution with initial pH 7, t = 22 ± 2 °C, the line is a second order kinetic model fit. B) Effect of background solution pH on sorption capacity (means ± standard deviation, n = 3), contact time = 24 h, t = 22 ± 2 °C.

Table 2. AIC values for kinetic and adsorption isotherm models.

	Kinetic models			Adsorption isotherm models	
Element	Biochar	Second order	First order	Hill model	Langmuir model
Pb	MSP550	-118.678	-128.926	157.149	157.760
	OSR550	-123.799	-111.672	167.402	175.854
	OSR700	-97.746	-108.825	150.232	195.784
	SWP550	-86.932	-74.059	-	-
	WSP550	-137.935	-134.369	174.766	183.262
Cd	MSP550	-82.747	-61.051	76.527	76.990
	OSR550	-106.998	-82.130	119.097	131.950
	OSR700	-80.193	-67.331	79.58973	145.806
	SWP550	-89.405	-89.728	-	-
	WSP550	-83.848	-66.698	111.449	125.145
Zn	MSP550	-93.397	-87.825	56.463	54.486
	OSR550	-114.667	-98.404	58.295	67.439
	OSR700	-105.267	-95.211	74.830	100.986
	SWP550	-42.776	-39.922	-	-
	WSP550	-89.543	-81.0505	94.719	101.688

Note: the model for which AIC is minimal is the one that best describes the experimental data.

3.2.2. *Effect of media pH*

The pH of the synthetic soil pore water had a significant effect on the adsorption of Zn(II), Cd(II) and Pb(II) by the biochars (Figure 1B). The adsorption capacity of Pb(II) was significantly decreased above pH 5 ($p < 0.001$); the greatest adsorption capacity was observed between pH 6 to pH 7 for Cd(II) ($p < 0.001$) and between pH 5 to pH 8 for Zn(II) ($p < 0.001$). Biochar SWP550 had the lowest sorption capacity for Cd(II) and Zn(II) at all pH values tested ($p < 0.001$) and for Pb(II) at pH 4, 5, 7, 8 and 9 ($p < 0.001$). These results are supported by the chemical speciation predicted with Visual MINTEQ 3.1 (Figure 2), which indicates that soluble forms of Cd(II), Pb(II) and Zn(II) available to bind with biochar sorption sites enhanced sorption at specific pH ranges. As illustrated in Figure 2, soluble Cd(II) forms, Cd^{2+} (93%) and $CdCl^{+}$ (2.5%), dominate at pH 4–7, after which insoluble $Cd_4(OH)_6SO_4(_s)$ would form and finally be the dominant species at pH 9. Pb(II) would be mainly present as soluble Pb^{2+} (90-62 %) and $PbOH^{+}$ (0.02–10.2 %) at initial pH 4–6.5; insoluble $Pb(OH)_2$ would start to form at pH 6.75 and become dominant at pH > 8 (98%). Zn(II) would be present as Zn^{2+} (96%) at pH 4–7, after which insoluble $Zn(OH)_2$ would form and became the dominant species at pH 9. The decreased sorption capacity for Pb(II) above the initial pH 5 reflects the progressively reduced solubility of Pb(II) at increasing pH. Other authors have reported similar effects of pH on the PTE sorption capacity of biochars. For example, biochars prepared from pinewood and rice husk have maximum Pb(II) removal capacities at pH 5 (Liu and

Table 3. Second order kinetic model and Hill sorption model parameters for the adsorption of Cd(II), Pb(II) and Zn(II) onto biochars. Kinetics conducted at initial concentration 5 mg.L^{-1} and pH 7. Sorption isotherms with concentrations starting at 0.05 mg.L^{-1} to 50 mg.L^{-1} (Zn with pH 7.5 and Cd with pH of 6.5) and up to 85 mg.L^{-1} for Pb (pH 5), contact time = 24 h, t = 22 ± 2 °C. Values are parameters means ± standard deviation; different letters indicate significant differences in parameters between biochars grouped by element ($p < 0.05$; pairwise ONE-WAY ANOVA).

		Second order kinetic model		Hill sorption model		
Element	Biochar	k_2 (g.mg^{-1}.min^{-1})	Q_e (mg.g^{-1})	n	q_m (mg.g^{-1})	K_H (mg.L^{-1})
Pb	MSP550	0.8 ± 0.2 a	0.345 ± 0.003 a	0.7 ± 0.2 a	41 ± 8 a	1 ± 1 a
	OSR550	0.27 ± 0.03 b	0.348 ± 0.002 a	2.7 ± 0.7 b	46 ± 4 a	0.22 ± 0.03 b
	OSR700	0.19 ± 0.03 c	0.368 ± 0.005 c	3.2 ± 0.3 b	56 ± 1 b	0.137 ± 0.005 c
	SWP550	0.10 ± 0.02 bc	0.344 ± 0.007 b	-	0.44*	-
	WSP550	0.53 ± 0.06 d	0.346 ± 0.001 a	2.1 ± 0.5 b	42 ± 3 a	0.19 ± 0.02 b
Cd	MSP550	0.079 ± 0.008 a	0.877 ± 0.007 a	1.4 ± 0.3 a	8.0 ± 0.7 a	2.6 ± 0.6 a
	OSR550	0.16 ± 0.01 b	0.882 ± 0.004 a	3.0 ± 0.8 b	19 ± 1 b	0.71 ± 0.06 b
	OSR700	0.068 ± 0.007 a	0.883 ± 0.008 a	6.4 ± 0.6 c	20.5 ± 0.5 b	0.335 ± 0.005 c
	SWP550	0.5 ± 0.4 d	0.089 ± 0.006 a	-	10.31*	-
	WSP550	0.13 ± 0.02 c	0.875 ± 0.007 a	6 ± 1 bc	18 ± 1 b	1.53 ± 0.06 a
Zn	MSP550	0.28 ± 0.05 a	1.070 ± 0.005 a	1.0 ± 0.5 a	3.3 ± 0.3 a	0.10 ± 0.06 a
	OSR550	0.36 ± 0.05 a	1.081 ± 0.003 a	1.6 ± 0.2 a	8.6 ± 0.3 b	0.068 ± 0.009 a
	OSR700	0.38 ± 0.07 a	1.046 ± 0.004 b	4.0 ± 0.6 b	10.7 ± 0.4 c	0.045 ± 0.002 b
	SWP550	0.06 ± 0.04 b	0.27 ± 0.03 ab	-	0.67*	-
	WSP550	0.4 ± 0.1 a	1.075 ± 0.006 a	4 ± 1 a	6.2 ± 0.6 a	0.034 ± 0.004 c

* Highest sorption capacity determined experimentally.

Zhang, 2009). The optimal pH for Zn(II) adsorption was determined to be pH 8 for hard wood biochar (Chen et al., 2011), pH 7 for Zn(II) adsorption by wheat straw biochar and pH 6 for Cd(II) on biochar made from *S. hermaphrodita* (Bogusz et al., 2015). The effect of pH on the sorption capacity of biochars differs for trace elements as solution pH significantly influences both metal speciation and biochar surface charge. Biochar addition increases the pH of the metal-enriched soil pore water solution. Due to release of alkaline mineral components and the presence of alkaline functional groups such as ketones on the biochar surface (Li et al., 2017; Waiapu and Mcmillan, 2018), an increase in solution pH enhances the formation of insoluble precipitates. This is especially important for Pb(II) as non-soluble forms start to develop at pH 6.75 according to the predicted speciation (Figure 2). Under acidic conditions the functional groups are protonated, but become deprotonated as pH increases, allowing binding of positively charged metal ions (Li et al., 2017). The enhanced sorption capacity for Cd(II) and Zn(II) at pH > 6 can be attributed to metal binding with deprotonated functional groups such as carboxylic (pKa 4.7–10.10) or acid-lactone (pKa 6.4–10.3), which are often present in biochars (Mandal et al., 2017).

Based on these findings the remaining sorption experiments were completed at an initial pH 5 for Pb(II) sorption, pH 6.5 for Cd(II) and pH 7.5 for Zn(II) to ensure maximum sorption capacity.

3.2.3. Sorption isotherms

Isotherm fitting in Figure 3 indicated that Langmuir and Hill are the sorption isotherm models that best described the experimental data. The Hill isotherm model was selected over the Langmuir model as fitting the experimental data better, based on AIC values (Table 2). The Hill isotherm describes the binding of different species by cooperative sorption mechanisms onto different substrates (Ayawei et al., 2017), including carbonaceous materials (Shahbeig et al., 2013). The cooperative binding is characterized by a side-by-side association between adsorbed molecules at low solute concentrations, while at higher solute concentrations there is progressively less chance that a solute molecule will find an available site (Giles et al., 1960). When the Hill coefficient of sigmoidicity $n > 1$ there is cooperative binding; while $n = 1$ indicates reactions of no cooperativity (Weiss, 1997). The n values derived from the Hill isotherms (Table 3) indicated cooperative binding in the adsorption of PTEs for all biochars except MSP550 with Pb(II). The cooperative sorption was confirmed by the sigmoidal "S"-shape isotherms observed at low equilibrium concentrations for Cd(II) and Pb(II) sorption with OSR550, OSR700 and WSP550 (Figure 4). This is important as bioavailable concentrations of PTEs in polluted soils are generally below 5 mg.L^{-1} (Berkowitz et al., 2014). "L"-shape isotherms, according to the isotherm classification of Giles et al. (1960), were observed for all PTEs with MSP550 and for all biochars with Zn(II) (Figure 4). The parameters derived from the Hill sorption model in Table 3 indicated that the maximum sorption capacities (q_m) were higher for Pb(II), followed by Cd(II) and Zn(II) (Pb > Cd > Zn). This trend is the same as that presented by Park et al. (2016), who obtained sorption capacities in the order Pb > Cd > Cr > Cu > Zn for sesame straw biochar applied at a rate of 2 g.L^{-1} in mono-metal systems when testing concentrations from 0 to 320 mg.L^{-1} at pH 7.

Biochar maximum sorption capacities (q_m) were, ordered from high to low, OSR700 > OSR550 > WSP550 > MSP550 > SWP550 for all PTEs tested. For Cd(II), biochar MSP550 (8 mg.L^{-1}) had a significantly lower ($p < 0.05$) sorption capacity than biochars OSR550 (19 mg.L^{-1}), OSR700 (21 mg.L^{-1}) and WSP550 (18 mg.L^{-1}). For Pb(II), biochar OSR700 (56 mg.L^{-1}) had a significantly higher ($p < 0.05$) sorption capacity than OSR550 (46 mg.L^{-1}), WSP (42 mg.L^{-1}) and MSP550 (41 mg.L^{-1}). For Zn(II) biochar OSR700 (11 mg.L^{-1}) demonstrated a significantly higher sorption ($p < 0.05$) capacity than OSR550 (9 mg.L^{-1}), WSP550 (6 mg.L^{-1}) and MSP550 (3 mg.L^{-1}). Overall herbaceous-derived biochars had a higher sorption capacity than the soft wood-derived biochar SWP550. Sun et al. (2014) also reported that four herbaceous biochars produced at 600 °C (corn, cotton, wheat and rice straw) had greater sorption capacity for Cd(II) than wood-derived biochar (poplar) produced at the same temperature. This was attributed to the limited pore development of the wood char due to the higher lignin content of wood. Trakal et al. (2014) concluded that "high lignin biomass" biochars are less effective than herbaceous biochars for Cd(II) and Pb(II) sorption, despite their high BET surface area.

Since K_H is the concentration of adsorbate (C_e) at half maximum sorption capacity (q_m), a biochar with a high K_H would require a greater concentration of adsorbate to achieve q_m, which implies a low affinity for the adsorbent, while low K_H values indicate that less concentration of adsorbate is required to achieve q_m, which represents a higher affinity between the adsorbate and biochar. Values of the Hill constants (K_H)

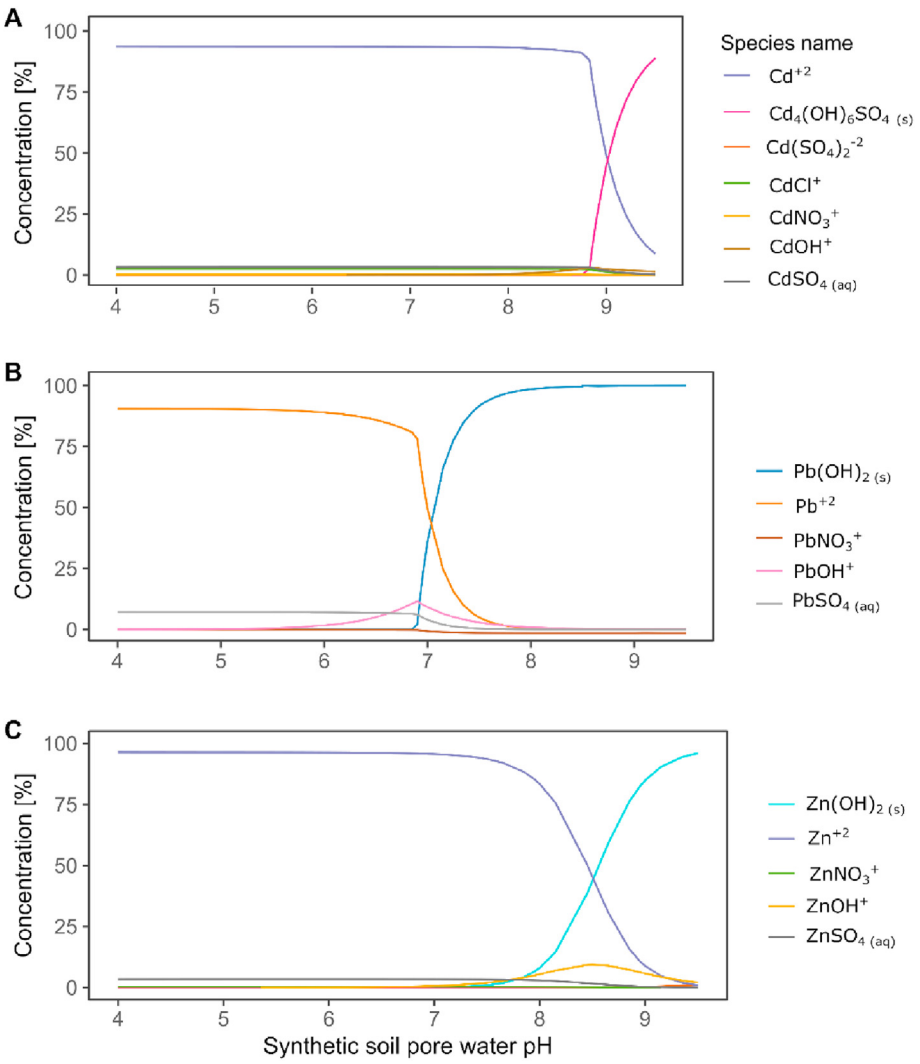

Figure 2. Inorganic speciation of studied elements in synthetic soil pore water. A) Cd(II), B) Pb(II), C) Zn(II). t = 22 °C and a total concentration of 5 mg.L^{-1} of each element.

shown in Table 3 indicate binding affinity in the order Zn(II) >Pb(II) >Cd(II) for all biochars. Although the binding affinity (K_H) of Zn(II) to all biochars was greatest, the sorption capacity (q_m) for this metal was the lowest. This indicates that Zn sorption is associated with less abundant, but high-affinity binding sites, whereas Cd(II) and Pb(II) sorption onto biochar is related to lower affinity, but more abundant binding sites. Other studies have reported that most Cd(II) sorption onto plant-derived biochars involves low binding energy sites (Cui et al., 2016b). Pourret and Houben (2018) characterized biochar binding sites using rare earth elements, indicating that strong aromatic functional groups, such as carboxy-phenolic and phenolic groups, have high affinity for metals while carboxylic groups have lower affinity.

3.3. Nature of sorption interactions

3.3.1. Functional groups analysis

Figure 5 illustrates the ATR-FTIR spectra of biochars with and without PTEs. Band positions and their assignments were identified according to major spectra structure correlations by spectral regions. Bands at 458 cm^{-1} were assigned to inorganic silicates Si–O asymmetric deformation vibration (Babu et al., 2011; Colthup et al., 1990). Si species present in biomass undergo changes during pyrolysis, where some of the Si species would transform into quartz, dehydroxylated silicates or alkali silicates (Qian et al., 2016). The band at 570 cm^{-1} was assigned to dicalcium phosphate or phosphate ion (PO_4^{3-}) bending (Bekiaris et al., 2016; Colthup et al., 1990). The change in the intensity of these bands in relation to the raw biochar was observed for all PTEs, however the changes in the band at 570 cm^{-1} associated with (PO_4^{3-}) bending were more pronounced after Zn(II) sorption. These shifts in the spectrum suggest the formation of Si complexes or Si mineral precipitates and phosphate precipitates with the trace element species calculated to be the dominant ones (Cd^{2+}, Pb^{2+} and Zn^{2+}). Changes of intensity and displacement of bands between 600 and 900 cm^{-1} were attributed to bending vibrations (CH) of aromatic groups. For instance, a band at 680 cm^{-1} (CH deformation) appeared in the spectra of biochars OSR550, WSP550 and MSP550 after Pb(II) exposure, suggesting an important role in the sorption of this PTE. Bands at 750, 780 and 870 cm^{-1} (CH bending) showed changes in intensity after exposure to all trace elements tested.

The aromatic structure of biochar surfaces may have promoted PTE sorption via cation–π bonding mechanisms, since aromatic structures have a pool of π electrons which can be donated to metal ions, thereby creating such interactions (Bandara et al., 2017). An abundance of lone-pair electrons is known to be associated with the "graphene-like" domains of plant-derived biochars (Harvey et al., 2011). Plant-derived biochars have been reported to immobilize Cd(II) (Cui et al., 2016a; Harvey et al., 2011), Pb(II) (Wang et al., 2015) and Zn(II) (Xu et al., 2013) by cation-π bonding mechanisms. This cation- π interactions can be considered an electrostatic effect that involves non-covalent bonding

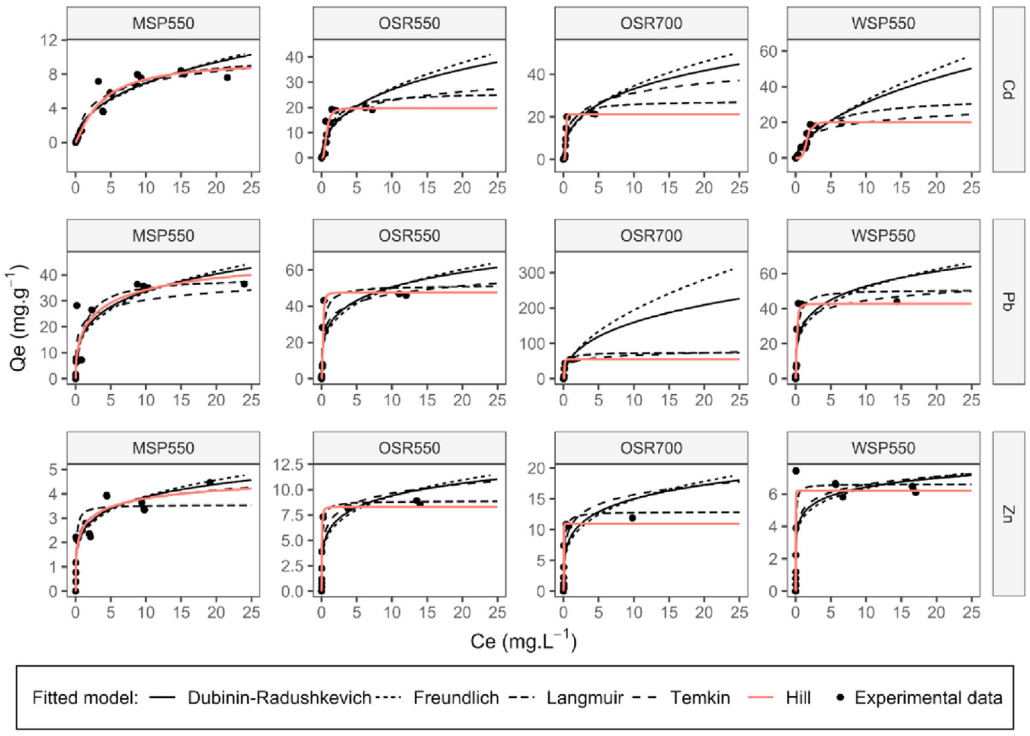

Figure 3. Adsorption isotherms of Cd(II), Pb(II) and Zn(II) fitted with the Dubinin-Radushkevich, Freundlich, Langmuir, Temkin and Hill sorption models. Biochar dose 1.25 g.L^{-1}, the initial pH of the background solution was pH 5 for Pb(II), pH 6.5 for Cd(II) and pH 7.5 for Zn(II) with a contact time of 24 h and t = 22 ± 2 °C.

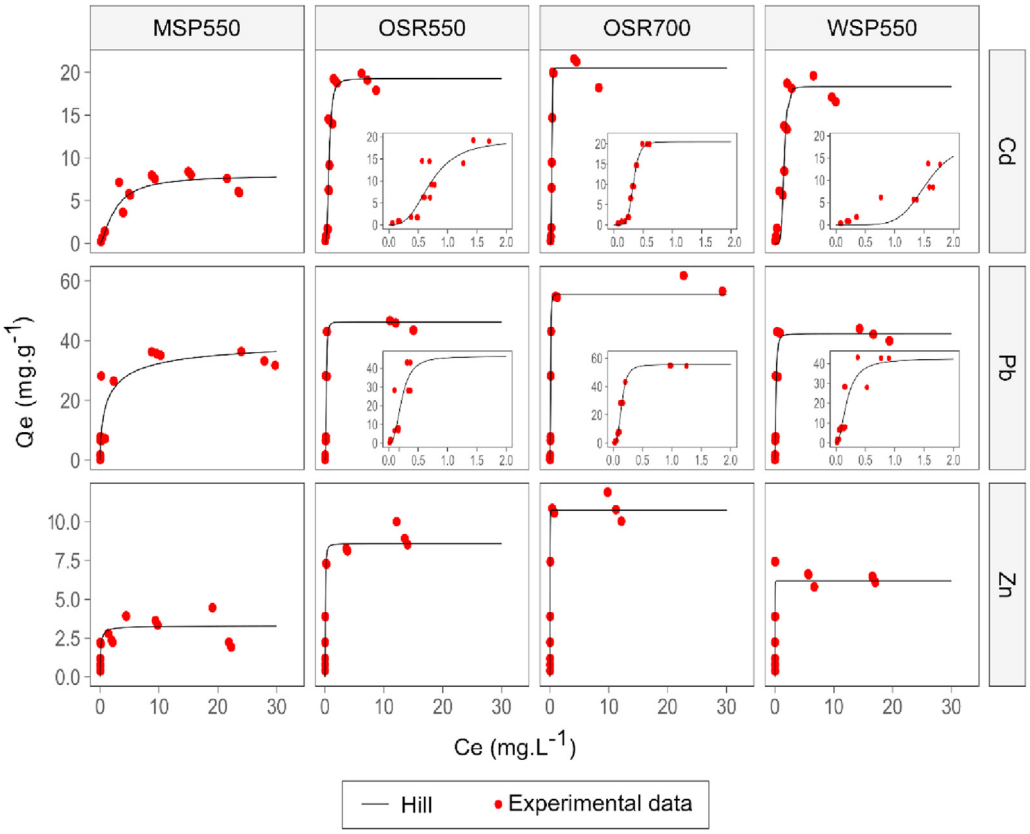

Figure 4. Adsorption isotherms for Cd(II), Pb(II) and Zn(II) fitted with the Hill sorption model. Inset plots, are close-ups that illustrate the sorption behaviour at equilibrium concentrations up to 2 mg.L^{-1}.The initial pH of the background solution was 5 for Pb(II), 6.5 for Cd(II) and 7.5 for Zn(II); 24 h contact time, t = 22 ± 2 °C.

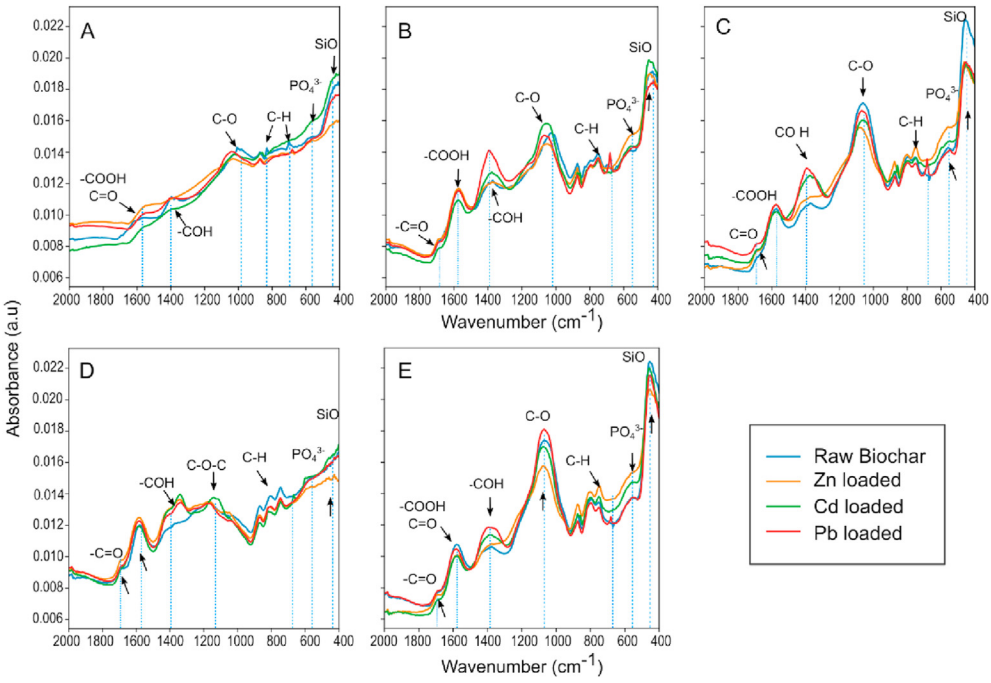

Figure 5. ATR-FTIR normalized spectra of biochars before and after sorption of Cd(II), Pb(II) and Zn. A) biochar OSR700, B) OSR550, C) WSP550, D) SWP550, E) MSP550.

between the quadrupole moment of the aromatic structure and the monopole of the cation, which allow aromatic systems to interact strongly with cations (Dougherty, 1996). The proposed mechanism for cation-π bonding between biochar aromatic structures and the studied metals is represented in Figure 6A.

The vibrations involving the asymmetric stretching of the C–O bond of aromatic secondary alcohols (phenyl–CHOH–) produced a strong band between 1000 to 1075 cm^{-1}. In OSR700 this band was absent, which is consistent with a higher pyrolysis temperature for this biochar. The loss of the 1030 cm^{-1}peak has been associated with higher production

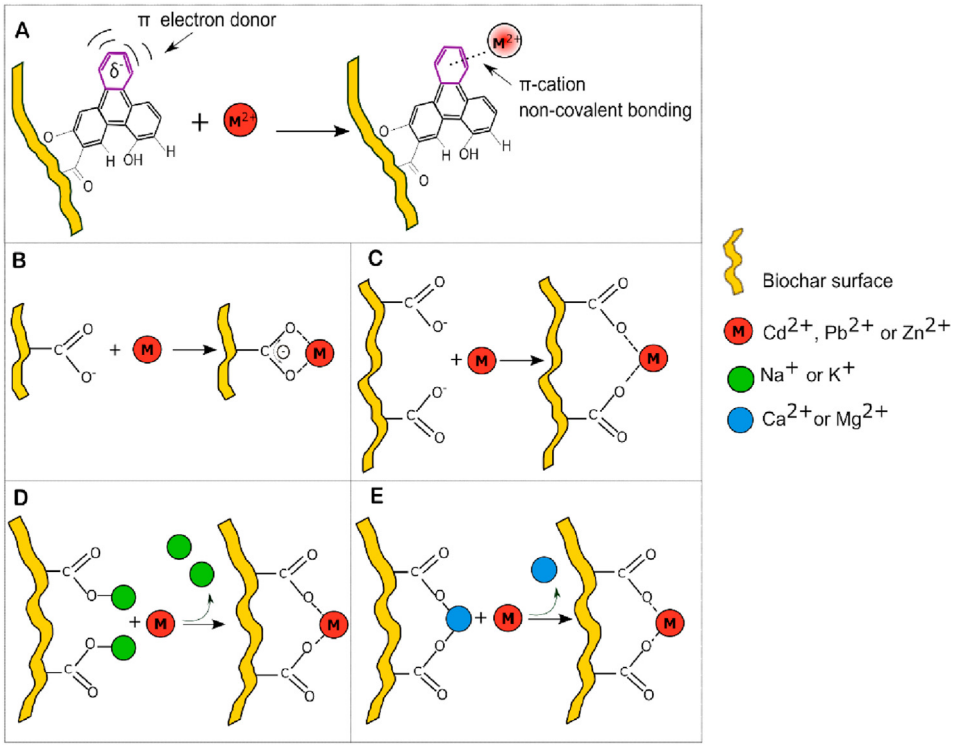

Figure 6. Biochar sorption mechanisms for Cd^{2+}, Pb^{2+} or Zn^{2+}. A) Cation–π interaction, B) Carboxylic group acting as a chelating ligand, C) Carboxylic groups forming a complex with a divalent cation. Surface complexation mediated by cation exchange of D) monovalent cations K^{+} or Na^{+} and E) divalent cations Ca^{2+} or Mg^{2+}.

temperatures due to dehydration, decarbonylation, and decarboxylation reactions (Uchimiya et al., 2011; Yang et al., 2007). The band was also absent in the spectra of the wood derived biochar SWP550. This was associated with the feedstock type; as presented by Domingues et al. (2017) the spectrum of lignocellulosic biochars were characterized by a weak peak or the complete absence of a band in this position. For the other biochars shifts in the intensity of this band and displacements to the left were observed after exposure to all PTEs. For biochar SWP550 a band between 1160-1200 cm^{-1} associated with C–O–C stretching of pyranose ring structures (Lazzari et al., 2018; Yang et al., 2007) increased in intensity after Cd(II) sorption. The band at 1380-1420 cm^{-1} was associated with phenols in solid state, which typically absorb between 1330-1390 cm^{-1} due to interaction between OH deformation and C–O stretch (Colthup et al., 1990) or to a δ (C–H) vibration in alkanes and alkyl groups (Komnitsas and Zaharaki, 2016). This last band indicated important shifts in intensity especially after contact with Cd(II) and Pb(II) for all the biochars. Bands attributed to metallic salts made from carboxylic acids (COO^-) were identified, the C=O and C–O bonds replaced by two equivalent carbon-oxygen bonds created a strong asymmetric COO stretching vibration at 1590 cm^{-1}. The carboxyl dimer infrared band of C=O stretch was identified at 1690 cm^{-1} (Ma et al., 2016). These bands associated with carboxylic groups are demonstrated to have an important role in the immobilization of the studied metals, especially for Pb(II) and Cd(II). The intensification of the bands may be attributed to chelation reactions between carboxylic acids and PTEs on biochar surfaces during the adsorption process, suggested by Wu et al. (2017) to be the dominant adsorption mechanism for Pb(II) on biochar. The coordination between oxygenated functional groups (e.g.,–COOH and–OH) and different heavy metals is usually accompanied with the release of H^+, resulting in the reduction of solution pH (Qian et al., 2016; Wang et al., 2015). In this study the solution pH during sorption was not controlled; samples containing low initial concentrations of PTEs had pH values at equilibrium of >8, >7 and >8 for Cd(II), Pb(II) and Zn(II) respectively (Figure 7), caused by the release of the mineral ash of biochars (Wang et al., 2015). However, as the concentration of PTEs in the solution increased, the pH of the solution decreased to <7.5, <7, <7.75 for Cd(II), Pb(II) and Zn(II), respectively, indicating that higher amounts of trace elements in the solution enhance the formation of complexes with oxygen-containing functional groups. These results were in accordance with Trakal et al. (2014) who reported a decrease of solution pH, particularly at higher PTE concentration and greater adsorption capacity. Samples treated with biochar SWP550, which is characterized by low ash content (Table 1), did not alter the solution pH (Figure 7).

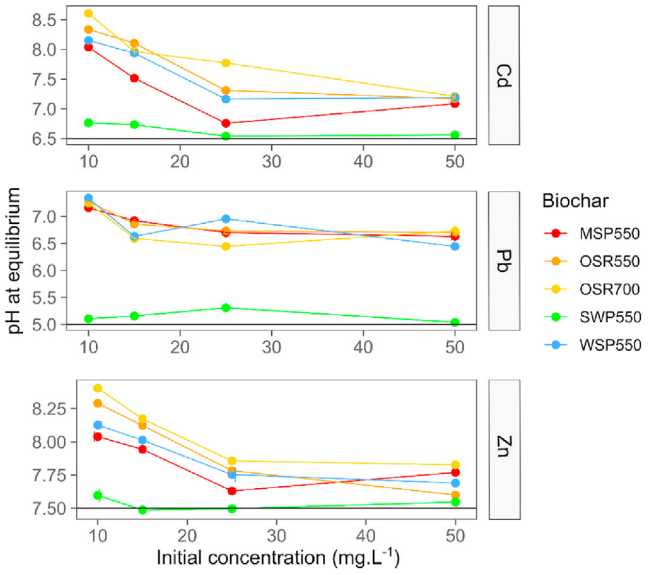

Figure 7. pH values at equilibrium at different trace element initial concentrations. A) Cd(II), B) Pb(II) and C) Zn(II). The black line — represents the initial pH of the soil pore water solution before being in contact with biochar. The biochar rate was 1.25 $g.L^{-1}$ in all samples, temperature was 22 ± 2 °C, contact time = 24 h. Values are the mean ± standard deviation, n = 3.

The complexation of PTEs with biochar surface functional groups has been schematized in Figure 6B-E, where complexation with deprotonated functional groups (chelation mechanism with carboxylic groups) or cation exchange-mediated complexation are represented.

The principal component analysis (PCA) of biochar spectra in Figure 8A shows that 68 % of the variation in the biochar spectra were explained by PC1 and 18 % by PC2. Feedstock origin and temperature significantly influenced biochar spectra ($p < 0.001$). In the PCA similar samples appear as clusters in the score plot, while different samples are segregated from each other. Biochar clustered as three groups: group one with biochar SWP550 samples (wood-derived biochar produced at 550 °C), group 2 with biochar samples WSP550, OSR550 and MSP550 (herbaceous biochars produced at 550 °C) and group 3 with OSR700 samples (herbaceous biochar produced at 700 °C). Biochars with fewer oxygen-functional groups (OSR700 and SWP550) were more distant from the other biochars. The bands responsible for the differentiation of these biochar groups are illustrated in Figure 8B and identified as carboxylic (COOH, C=O), phenolic (COH, C–O), aromatic (C–H), PO_4^{3-} and SiO.

3.3.2. Scanning electron microscopy with energy dispersive X-ray spectroscopy

Visual comparison of SEM-EDX images using biochar MSP550 (Figure 9) demonstrates the typical effect of PTE exposure on pores and mineral phases at the biochar surface. The SEM-EDX images of the other four biochars can be accessed at Soria et al. (2020). SEM backscattered images revealed a heterogeneous topography and material contrasts (composition). PTE immobilization was confirmed on biochar surfaces; elements with higher atomic number such as Pb(II), Cd(II) and Zn(II) yield more backscattered electrons, which appear brighter on the image (left column on Figure 9).

Electronic x-ray mapping was used to visualize the colocalization of elements on SEM images of biochar MSP550 loaded with PTEs. The images show colocalization of Si and O, indicating the presence of compounds containing Si minerals on the biochar surface. The images also show that Cd(II) occurred together with K^+, suggesting compounds containing Cd^{2+} and K^+. The formation of K_4CdCl_6 precipitates has been previously reported on Cd-loaded biochars (Bashir et al., 2018; Xu et al., 2017; Zhang et al., 2015). Likewise, the images revealed that Pb(II) occurred together with S. In other studies precipitates of Pb(II) with sulphate compounds such as $Pb_2(SO_4)O$ and $Pb_4(CO_3)_2(SO_4)(OH)_2$ have been reported to contribute to Pb(II) metal sorption (Wang et al., 2015). Regarding Zn(II)-loaded samples, there was no clear indication of elements occurring at the same positions as Zn(II), apart from O, for any biochar analysed.

These SEM-EDX results suggest that in the case of Cd(II) and Pb(II), in addition to the interactions with functional groups indicated in section 3.3.1, sorption could have also be mediated by the formation of mineral precipitates containing K^+ and S.

3.3.3. Competitive sorption

The effect of metal competition on the sorption capacity of biochars in binary and ternary equimolar systems is illustrated in Figure 10. The presence of additional elements in synthetic soil pore water had a significant effect ($p < 0.001$) on the sorption capacity of the biochars for PTEs. In the systems containing equimolar concentrations of Zn(II) and Cd(II) the sorption capacity for Zn(II) was higher than for Cd(II) ($p < 0.05$) for all the biochars. When Pb(II) was present, either in Zn-Pb or Pb-Cd binary systems, or the ternary system containing Pb(II), Cd(II) and Zn(II); the sorption capacity for Pb(II) was significantly higher ($p < 0.001$), limiting the binding of the other elements for all the biochars. The higher sorption capacity for Pb(II) in the multi-element sorption studies regardless of the biochar type is consistent with the higher

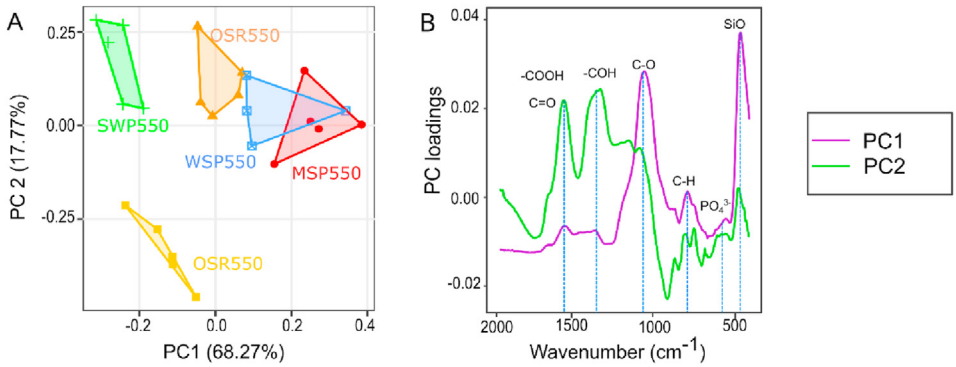

Figure 8. Principal component analysis (PCA) of normalized ATR-FTIR spectra of plant-based biochars. A) Score plots of PC1 and PC2, B) PC loadings against the wavenumber indicating the bands that mostly contributed to the separation of biochar groups in the PCA.

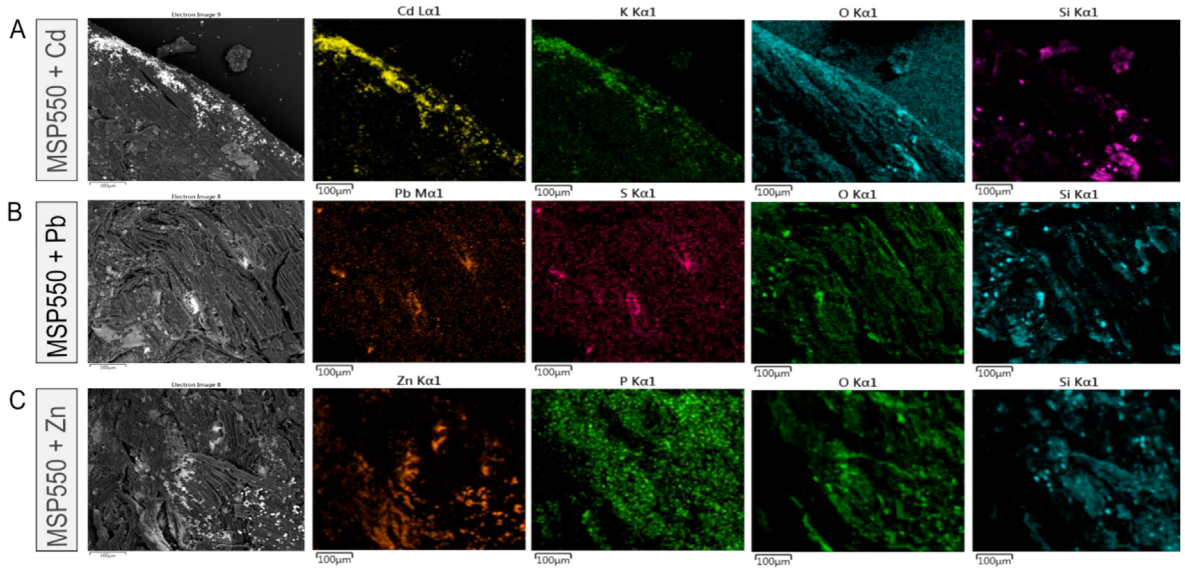

Figure 9. SEM-EDX images of biochar MSP550 after sorption of Cd, Pb and Zn and the main elements identified on its surface.

sorption capacity for Pb(II) observed in the mono-element sorption studies (section 3.2.3). This finding is supported by the results of Park et al. (2016), who reported a sorption capacity in the order of Pb > Cu > Cr > Zn > Cd for a multi-element sorption experiment using sesame straw biochar. These results are consistent with our findings and indicate that in spite of a lower Zn(II) sorption capacity (Zn < Cd) in mono-metal systems, Zn(II) sorption was higher than Cd(II) (Zn > Cd) when in competition.

The negligible sorption of Zn(II) or Cd(II) in the presence of Pb(II) suggests that these trace elements compete for the same sorption sites. The sorption of PTEs onto biochar depends on the nature of the elements involved. The adsorption preference exhibited by biochars for Pb(II) over Zn(II) and Cd(II) when in competition could be due to (i) the hydrolysis constant, (ii) the ionic radius, and subsequently hydrated radius, and (iii) its Misono softness value due to a stronger surface electrostatic attraction. The first hydrolysis constant (pK) of Pb^{2+} (7.71) is lower than that of Cd^{2+} (10.1) and Zn^{2+} (9.0) (Park et al., 2016). The first hydrolysis product of divalent ions is capable of forming complexes with the adsorbent, which result in stronger element retention (inner-sphere complexes) than the electrostatic attraction of hydrated ion elements. Thus, the lower the hydrolysis constant of the element, the stronger the element specific sorption (Shaheen et al., 2013). Pb^{2+} has a smaller hydrated radius of 4.01 Å compared with Cd^{2+} (4.26 Å) or Zn^{2+} (4.30 Å). The larger the hydrated radius the higher the activation energy required to initiate cation exchange (Harvey et al., 2011), besides a smaller hydrated radius favours Coulombic interactions (outer-sphere complexes) between the cation and exchange sites of the adsorbent (Shaheen et al., 2013). The scale of Misono represents the acidity of metal ions as Lewis acids based on two parameters, one associated with the softness and the second to the electronegativity of the ion. Considering these two parameters respectively, Pb^{2+} (3.58, 4.15) is a harder acid than Zn^{2+}(2.34, 4.64), while Cd^{2+} (3.04, 4.60) is considered a soft acid (Misono et al., 1967). According to the HSBA theory (Alfarra et al., 2004), as a harder acid Pb(II) would have greater affinity than Zn(II) or Cd(II) for the carboxylic functional groups (band at 1590 cm^{-1}) and phenolic groups (band 1380-1420 cm^{-1}) identified on biochars, which are hard Lewis bases. Thus, the preferential retention of Pb(II) to Zn(II) or Cd(II) is in agreement with differences in ionic radius, first hydrolysis constants, and the Misono softness parameter, making Pb(II) a better candidate than the other elements for both electrostatic and inner-sphere surface complexation reactions. The same reasoning can be applied to explain Zn(II) preferential sorption over Cd(II), in that the first hydrolysis constants as well as the Misono scale and the HSBA theory accurately predict the observed sequence Zn(II) > Cd(II), however the hydrated ionic radius reasoning predicts Cd(II) > Zn(II) which is the opposite of the results obtained. This suggests that Zn(II) vs Cd(II) competitive sorption was not entirely electrostatic, since elements with larger ionic radius would have been sorbed less strongly (Shaheen et al., 2013), which was not the case. Other authors have suggested that the hydrolysis constant may be a good predictor of selective element retention rather

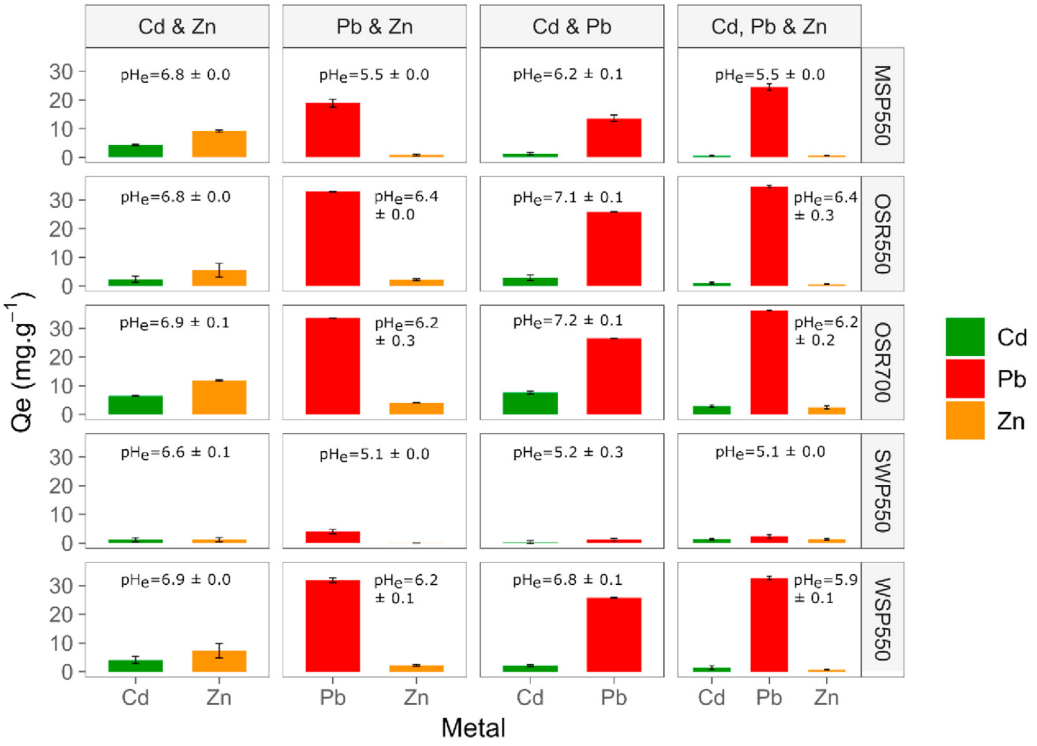

Figure 10. Competitive sorption of PTEs onto biochar using binary and tertiary systems. Initial concentrations were for Zn(II) 13 mg.L^{-1}, Pb(II) 41 mg.L^{-1} and Cd(II) 22 mg.L^{-1} which equals 0.2 mM of each metal. Contact time = 24 h, t = 22 ± 2 °C. Results are the average of 3 measurements ±standard error. Initial pH 6.5 for binary system Zn-Cd and pH 5 for the rest of combinations; pH_e is the pH value at equilibrium ±standard error.

than the Misono (HSBA theory) or the ionic radius (Park et al., 2016; Shaheen et al., 2013).

PTEs in polluted soils are usually present as mixtures and their interactions are known to influence their transport and fate between phases (Chen et al., 2011; Park et al., 2013). Therefore, it is important to conduct competitive sorption tests. The results indicate that in a scenario where Pb(II), Cd(II) and Zn(II) coexist in a polluted soil, regardless of the type of biochar applied as a remediation measure, the adsorbent will preferentially immobilize Pb(II) over the other elements, requiring a higher biochar application rate to maximize binding of additional PTEs.

3.4. Linking biochar properties to PTEs immobilization

The Pearson correlation analysis illustrated in Figure 11A indicated that CEC, pH, electric conductivity (EC) and total K^+ were highly correlated (>0.8) with Cd(II) sorption capacity (q_{mCd}). Pb(II) sorption capacity (q_{mPb}) was highly correlated (>0.8) with pH, CEC, EC and total P. Zn(II) sorption capacity (q_{mZn}) had a correlation coefficient of 1.0 with EC and >0.8 with pH, total P and total K. The high correlations between biochar sorption capacities (q_m) and CEC, EC and biochar pH suggest that the PTE sorption is dominated by electrostatic interactions and precipitation mechanisms. This implies that the surface complexes formed with Cd(II), Pb(II) and Zn(II) on biochars are mainly outer-sphere complexes. This is in agreement with the speciation diagram (Figure 2) which indicated that for the range of pH found at equilibrium (Figure 7), the dominant trace element species would be the free cation species Cd^{2+} (96 %), Pb^{2+} (95-81 %) and Zn^{2+} (96-83 %), while the hydrolysed forms $CdOH^+$ (0.5 %), $PbOH^+$ (3–10%) and $ZnOH^+$ (2–5%) that enhance inner-sphere complexes formation are expected in smaller amounts. It is important to highlight that outer- and inner-sphere complexation can occur simultaneously (Sparks, 2003). Our findings are similar to that of Trakal et al. (2014), who reported a high correlation between Cd(II) and Pb(II) removal and the CEC and pH of various biochars, although they did not consider EC, biochar mineral constituents or functional groups.

The high correlation of q_{mPb} and q_{mZn} with total P and EC is supported by the ATR-FTIR analysis, where shifts in the intensity of PO_4^{3-} were observed after contact with Zn(II), but also Pb(II). This implies that formation of precipitates with soluble phosphates released from biochar contributes to Pb(II) and Zn(II) immobilization. Previously the formation of phosphate precipitates with Pb(II) such as $Pb_5(PO_4)_3OH$ (Cao et al., 2009), $Pb_3(PO_4)_2$ (Wu et al., 2017) or Zn(II) precipitates such as $Zn_3(PO_4)_2$ (Qian et al., 2016) or $Zn_3(PO_4)_2.4H_2O$ (Xu et al., 2013) have been reported on biochar surfaces. Furthermore, the high correlation of q_{mZn} with EC and total K^+ suggests the interaction of Zn(II) with soluble minerals containing K^+ as an important contributor in Zn(II) immobilization. The formation of large amounts of hemimorphite ($Zn_4(Si_2O_7)(OH)_2{\cdot}H_2O$) mediated by soluble K_2SiO_3 released from wheat straw biochar produced at 550 °C was reported by Qian et al. (2016) as one of the main Zn(II) sorption mechanisms. The interaction of Zn(II) with Si-O and PO_4^{3-} groups observed in the ATR-FTIR analysis of Zn(II)-loaded biochars is in agreement with the direct correlation between EC and q_{mZn}., implying that besides the observed interaction of Zn(II) with oxygenated functional groups (phenolic and carboxylic), another important mechanism for Zn(II) immobilization was precipitation with phosphate and silicate soluble minerals.

The high correlation of q_{mCd} with total K^+ and CEC suggests the occurrence of cation exchange mechanisms between Cd(II) and K^+ by electrostatic ion exchange with surface functional groups of biochar or with K^+ present in biochar minerals.

The EC values (dS.m^{-1}) indicate the amount of biochar water-soluble salts (Jiang et al., 2017). Soluble cations and anions released from biochar can show a strong positive correlation with CEC and anion exchange capacity (AEC) (Xu et al., 2017), both mechanisms associated with Pb(II), Zn(II) and Cd(II) immobilization by biochar (Komkiene and Baltrenaite, 2016; Lu et al., 2012; Ma et al., 2016). The adsorption affinity of water-soluble mineral fractions in biochar for PTEs is much higher than that of water-insoluble minerals (Xu et al., 2017). For instance, soluble cations including potassium (K^+), calcium (Ca^{2+}), magnesium (Mg^{2+}),

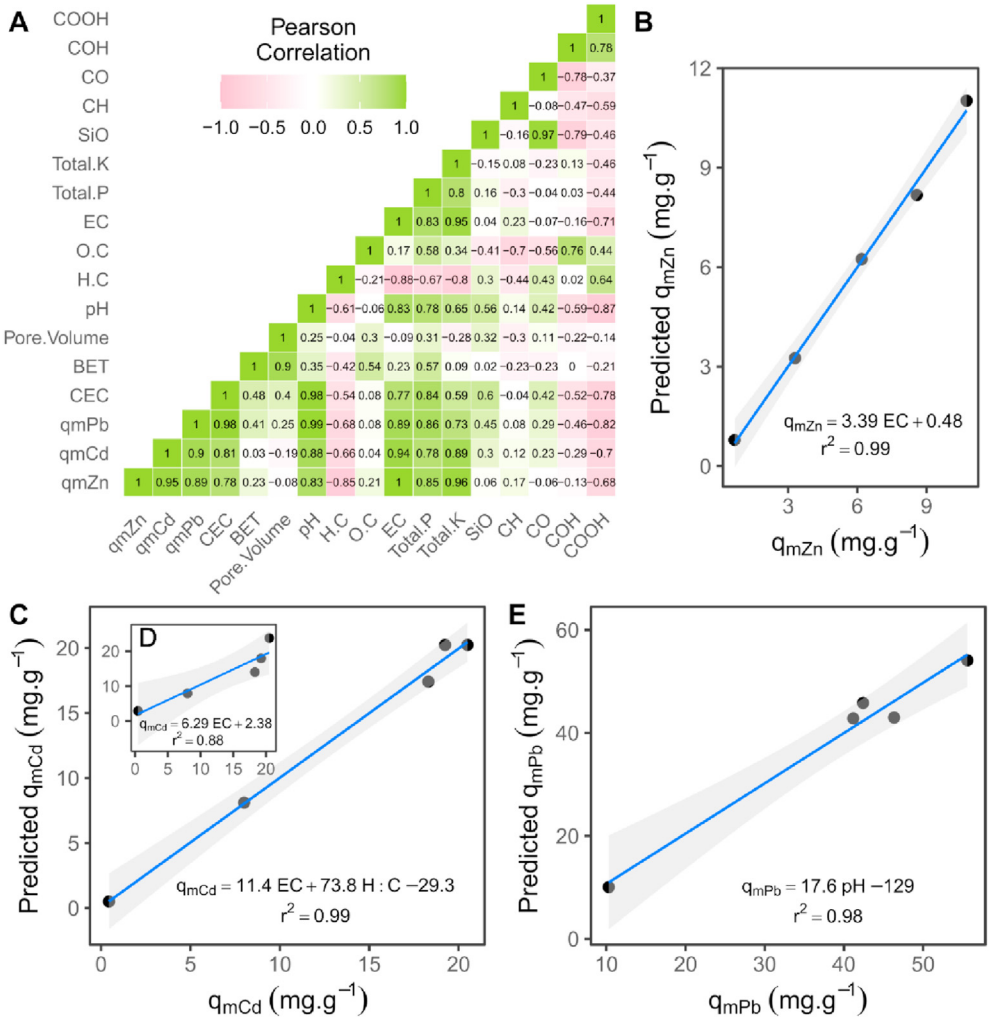

Figure 11. Relationship between biochar sorption performance and physico-chemical properties. A) Pearson correlation matrix betweenphysico-chemical properties of biochar and sorption capacity q_m (mg.g^{-1}) for Cd(II), Zn(II) and Pb(II). Plots showing predicted sorption capacity versus the maximum sorption capacity (mg.g^{-1}) observed for B) Zn with single variable linear regression, C) Cd multi variable linear regression, D) Cd single variable linear regression and E) Pb single variable linear regression. Blue lines are regression lines and grey areas indicate 95% confidence intervals for predicted biochar sorption capacity.

and anions (PO_4^{3-} or CO_3^{2-}) in biochar participate in ion exchange reactions or form precipitates with PTEs, reducing their availability (Li et al., 2017; Xu et al., 2017). Trakal et al. (2014) suggested the release of cations as the most important characteristic in biochar selection for metal sorption.

The high correlation between q_m and pH also reflects the importance of biochar mineral constituents; alkali metals (Na^+, K^+) or alkaline earth metals (Ca^{2+}, Mg^{2+}) in the form of carbonates are the main alkaline substances responsible for the high pH of biochar (Xu et al., 2017). Furthermore, higher pH values favour deprotonation of carboxylic and other functional groups, thus negatively charged sorption sites are created on the surface of all biochars (Trakal et al., 2014). Therefore, the high correlation of q_m with biochar pH suggests that a higher biochar pH is associated with a higher immobilization potential due to different mechanisms (complexation or precipitation). As per EC, these correlations suggest that biochars with a high soluble mineral content would have a higher pH, EC and CEC, supporting PTEs immobilization.

The low potential for Cd(II), Pb(II) and Zn(II) sorption on SWP550 can be related to the feedstock type. Wood-derived biochars, such as SWP550, are reported to have low EC values (Domingues et al., 2017), whereas crop-derived biochars often exhibit greater EC values. This is consistent with SWP550, which has the lowest EC, CEC, ash content and pH.

No direct correlation between PTE sorption capacity and surface area (BET) was found. Previous studies have also reported a poor correlation between the surface areas of plant-derived biochars and Cd(II) (Sun et al., 2014), and Cd(II) and Pb(II) sorption capacities (Trakal et al., 2014). Similarly, no direct correlation was identified between sorption capacity (q_m) and the absorbance of the functional groups used in the correlation analysis despite their known role in sorption of PTEs. This indicates that there is no quantitative relationship between surface area and q_m and between functional groups and q_m, suggesting that the importance of these biochar properties is of a qualitative nature instead.

Overall, the correlation analysis highlighted the importance of the biochar water soluble mineral fraction as a potential indicator of PTE immobilization. The inherent mineral constituents in biochar may explain up to 90% of metal removal by biochars (Xu et al., 2017). In this respect EC, CEC and pH are properties of biochar that directly reflect PTE sorption potential and should be considered as the most important criteria when selecting a biochar for the remediation of soils polluted with Pb(II), Cd(II) and Zn(II). Consequently, herbaceous biochars may exhibit a greater potential for PTE immobilization as they are characterized by higher EC, CEC and pH than wood derived biochars.

3.5. Models describing PTE sorption potential

The models obtained to describe biochar sorption capacity for Cd(II), Pb(II) and Zn(II) as a function of biochar physico-chemical properties are presented in Table 4 and illustrated in Figure 11A. Pb(II) sorption (q_{mPb}) was described mainly as a function of biochar pH, as shown in Figure 11E. The sorption capacity for Zn(II) (q_{mZn}) was fully explained by

Table 4. Linear models which describe biochar sorption capacity (q_m) for Pb(II), Zn(II) and Cd(II).

PTE	Type of linear model	Graph	Coefficients	Estimate	Signif. codes	Multiple R^2	Adjusted R^2	F-statistic	p-value
Zn	Single variable[a]	Figure 6B	Intercept	0.5 ± 0.2		0.99	0.99	747	< 0.001
			EC (dS.m^{-1})	3.4 ± 0.1	***				
Pb	Single variable[a]	Figure 6E	Intercept	-129 ± 15	**	0.98	0.97	123	<0.01
			pH	18 ± 2	**				
Cd	Single variable[a]	Figure 6D	Intercept	2 ± 3		0.88	0.84	21.9	0.02
			EC (dS.m^{-1})	7 ± 2	*				
	Two variables[b]	Figure 6C	Intercept	-29 ± 5	*	0.99	0.99	163	0.01
			EC (dS.m^{-1})	11.4 ± 0.8	**				
			H.C (molar ratio)	74 ± 12	*				

*** = coefficients are significant 100%, ** = coefficients are significant 99.9 %, * = coefficients are significant 99%.
[a] formula, $y = mx + b$.
[b] formula, $y = m_1x_1 + m_2x_2 + b$.

the biochar EC (dS.m^{-1}) (Figure 11B.). For Cd(II) sorption (q_{mCd}) the best predictor was EC (dS.m^{-1}), however as illustrated in Figure 11D, the relationship was not linear. A second parameter (H:C ratio) was introduced into this regression which improved its linearity (Figure 11C.). The addition of H:C ratio as a predictor of Cd sorption implies that biochar aromaticity is related to Cd(II) immobilization mechanisms, which is consistent with results from the ATR-FTIR analysis.

4. Conclusions

Regardless of biochar type, the immobilization of Pb(II) was favoured over Cd(II) and Zn(II) in both single and competitive systems. The sorption between the studied PTEs and plant-based biochars was dominated by electrostatic interactions. Cd(II) and Pb(II) sorption was mediated by complexation with carboxylic groups mainly enhanced by cation exchange mechanisms, cation–π interactions and precipitation with biochar phosphates and silicates; while Zn(II) sorption was mediated by complexation with phenolic groups and precipitation with biochar phosphates. Statistical analysis showed that biochar sorption capacity was highly correlated with biochar properties EC, CEC and pH, which are associated with biochar water-soluble minerals. These results confirmed the hypothesis that the potential for PTE sorption by plant-based biochars can be predicted from a relatively limited suite of physico-chemical properties, which may facilitate the selection of biochars for the immobilization of PTEs in soils. Accordingly, biochars derived from herbaceous feedstock were demonstrated to be better candidates for the remediation of soil polluted with PTEs than wood-derived materials.

However, a limitation of this study is the small number of plant-based biochars analysed in relation to the wide variety of feedstock existing as well as the absence of dissolved organic matter as part of the synthetic soil pore water solution. Further research should focus on developing robust mathematical models to optimize estimates of biochar sorption capacity and application for different soil remediation scenarios. Predictive models are required to optimize soil restoration strategies which reduce biochar application costs by selecting the most suitable materials.

Author contribution statement

Rosa I. Soria: Conceived and designed the experiments; Performed the experiments; Analyzed and interpreted the data; Contributed reagents, materials, analysis tools or data; Wrote the paper.

Stephen A. Rolfe: Conceived and designed the experiments; Analyzed and interpreted the data; Contributed reagents, materials, analysis tools or data.

Mauro Pazmiño Betancourth: Performed the experiments; Contributed reagents, materials, analysis tools or data.

Steven F. Thornton: Conceived and designed the experiments; Analyzed and interpreted the data; Contributed reagents, materials, analysis tools or data.

Funding statement

This work was supported by the Marie Skłodowska-Curie Innovative Training Network INSPIRATION funded by the European Union's Horizon 2020 research and innovation programme (Grant agreement no. 675120).

Declaration of interest statement

The authors declare no conflict of interest.

Additional information

No additional information is available for this paper.

Acknowledgements

The authors acknowledge the support provided by the Groundwater Protection and Restoration Group (GPRG), the laboratory manager Andrew Fairburn, the Animal and Plant Sciences Department and the Sorby Centre of The University of Sheffield and the UK Biochar Research Centre for providing the biochar samples. Finally we thank three anonymous reviewers for critically reading the manuscript and suggesting substantial improvements.

References

Akaike, H., 1974. A new look at the statistical model identification. IEEE Trans. IEEE Trans. Automat. Contr. 19, 716–723.
Akpa, O.M., Unuabonah, E.I., 2011. Small-Sample Corrected Akaike Information Criterion: an appropriate statistical tool for ranking of adsorption isotherm models. Desalination 272, 20–26.
Alfarra, A., Frackowiak, E., Béguin, F., 2004. The HSAB concept as a means to interpret the adsorption of metal ions onto activated carbons. Appl. Surf. Sci. 228, 84–92.
Ayawei, N., Ebelegi, A.N., Wankasi, D., 2017. Modelling and interpretation of adsorption isotherms. J. Chem. 2017.
Babu, B.C., Naresh, V., Prakash, B.J., Buddhudu, S., 2011. Structural, thermal and dielectric properties of lithium zinc silicate ceramic powders by sol-gel method. Ferroelectrics Lett. 38, 114–127.
Bandara, T., Herath, I., Kumarathilaka, P., Hseu, Z.-Y., Sik Ok, Y., Vithanage, M., 2017. Efficacy of woody biomass and biochar for alleviating heavy metal bioavailability in serpentine soil. Environ. Geochem. Health 39, 391–401.
Bashir, S., Zhu, J., Fu, Q., Hu, H., 2018. Comparing the adsorption mechanism of Cd by rice straw pristine and KOH-modified biochar. Environ. Sci. Pollut. Res. 25, 11875–11883.
Bekiaris, G., Peltre, C., Jensen, L.S., Bruun, S., 2016. Using FTIR-photoacoustic spectroscopy for phosphorus speciation analysis of biochars. Spectrochim. Acta Part A Mol. Biomol. Spectrosc. 168, 29–36.

Berkowitz, B., Dror, I., Yaron, B., 2014. Contaminant Geochemistry: Interactions and Transport in the Subsurface Environment, second ed. 1–577.
Bogusz, A., Oleszczuk, P., Dobrowolski, R., 2015. Application of laboratory prepared and commercially available biochars to adsorption of cadmium, copper and zinc ions from water. Bioresour. Technol. 196, 540–549.
Cao, X., Ma, L., Gao, B., Harris, W., 2009. Dairy-manure derived biochar effectively sorbs lead and atrazine. Environ. Sci. Technol. 43, 3285–3291.
Caporale, A.G., Pigna, M., Sommella, A., Conte, P., 2014. Effect of pruning-derived biochar on heavy metals removal and water dynamics. Biol. Fertil. Soils 50, 1211–1222.
Chen, X., Chen, G., Chen, L., Chen, Y., Lehmann, J., McBride, M.B., Hay, A.G., 2011. Adsorption of copper and zinc by biochars produced from pyrolysis of hardwood and corn straw in aqueous solution. Bioresour. Technol. 102, 8877–8884.
Colthup, N.B., Daly, L.H., Wiberley, S.E., 1990. Introduction to Infrared and Raman Spectroscopy, Third. ed. Academic Press, Inc, San Diego, California.
Cui, X., Fang, S., Yao, Y., Li, T., Ni, Q., Yang, X., He, Z., 2016a. Potential mechanisms of cadmium removal from aqueous solution by Canna indica derived biochar. Sci. Total Environ. 562, 517–525.
Cui, X., Hao, H., Zhang, C., He, Z., Yang, X., 2016b. Capacity and mechanisms of ammonium and cadmium sorption on different wetland-plant derived biochars. Sci. Total Environ. 539.
Demsar, J., Curk, T., Erjavec, A., Gorup, C., Hocevar, T., Milutinovic, M., Mozina, M., Polajnar, M., Toplak, M., Staric, A., Stajdohar, M., Umek, L., Zagar, L., Zbontar, J., Zitnik, M., Zupan, B., 2013. Orange: data mining toolbox in phyton. J. Mach. Learn. Res. 14, 2349–2353.
Di Bonito, M., 2005. Trace Elements in Soil Pore Water : a Comparison of Sampling Methods. University of Nottingham.
Domingues, R.R., Trugilho, P.F., Silva, C.A., de Melo, I.C.N.A., Melo, L.C.A., Magriotis, Z.M., Sánchez-Monedero, M.A., 2017. Properties of biochar derived from wood and high-nutrient biomasses with the aim of agronomic and environmental benefits. PloS One 12, e0176884.
Dougherty, D.A., 1996. Cation-π interactions in chemistry and biology: a new view of benzene, Phe, Tyr, and Trp. Science (80-.) 271, 163–168.
Dubinin, M., 1975. Physical Adsorption of Gases and Vapors in Micropores. Elsevier, pp. 1–70.
Freundlich, H., 1906. Über die Adsorption in Lösungen. Z. Phys. Chem. 57 (1), 385–470.
Giles, C.H., Macewan, T.H., Nakhwa, S.N., Smith, D., 1960. A system of classification of solution adsorption isotherms, and its use in diagnosis of adsorption mechanisms and in measurement of specific surface areas of solids. J. Chem. Soc. 111, 3973–3993.
Giller, K.E., Witter, E., Mcgrath, S.P., 1998. Toxicity of heavy metals to microorganisms and microbial processes in agricultural soils: a review. Soil Biol. Biochem. 30, 1389–1414.
Goutelle, S., Maurin, M., Rougier, F., Barbaut, X., Bourguignon, L., Ducher, M., Maire, P., 2008. The Hill equation: a review of its capabilities in pharmacological modelling. Fundam. Clin. Pharmacol. 22, 633–648.
Harvey, O.R., Herbert, B.E., Rhue, R.D., Kuo, L.-J., 2011. Metal interactions at the biochar-water interface: energetics and structure-sorption relationships elucidated by flow adsorption microcalorimetry. Environ. Sci. Technol. 45, 42.
Hill, A.V., 1910. The possible effects of the aggregation of the molecules of haemoglobin on its dissociation curves. J. Physiol. 40, 4–7.
Ho, Y.S., McKay, G., 1998. Sorption of dye from aqueous solution by peat. Chem. Eng. J. 70, 115–124.
Hu, Q., Zhang, Z., 2019. Application of Dubinin–Radushkevich isotherm model at the solid/solution interface: a theoretical analysis. J. Mol. Liq. 277, 646–648.
Janus, A., Pelfrêne, A., Heymans, S., Deboffe, C., Douay, F., Waterlot, C., 2015. Elaboration, characteristics and advantages of biochars for the management of contaminated soils with a specific overview on Miscanthus biochars. J. Environ. Manag. 162, 275–289.
Jiang, S., Nguyen, T.A.H., Rudolph, V., Yang, H., Zhang, D., Ok, Y.S., Huang, L., 2017. Characterization of hard- and softwood biochars pyrolyzed at high temperature. Environ. Geochem. Health 39, 403–415.
Keiluweit, M., Nico, P.S., Johnson, M., Kleber, M., 2010. Dynamic molecular structure of plant biomass-derived black carbon (biochar). Environ. Sci. Technol. 44, 1247–1253.
Kinniburgh, D.G., Miles, D.L., 1983. Extraction and chemical analysis of interstitial water from soils and rocks. Environ. Sci. Technol. 17, 362–368.
Komkiene, J., Baltrenaite, E., 2016. Biochar as adsorbent for removal of heavy metal ions [Cadmium(II), Copper(II), Lead(II), Zinc(II)] from aqueous phase. Int. J. Environ. Sci. Technol. 13, 471–482.
Komnitsas, K.A., Zaharaki, D., 2016. Morphology of modified biochar and its potential for phenol removal from aqueous solutions. Front. Environ. Sci. 4, 1–11.
Lagergren, S., 1898. Zur theorie der sogenannten adsorption geloster stoffe. Kungliga Svenska Vetenskapsakademiens.
Langmuir, I., 1918. The adsorption of gases on plane surfaces of glass, mica and platinum. J. Am. Chem. Soc. 40, 1361–1403.
Lazzari, E., Schena, T., Marcelo, M.C.A., Primaz, C.T., Silva, A.N., Ferrão, M.F., Bjerk, T., Caramão, E.B., 2018. Classification of biomass through their pyrolytic bio-oil composition using FTIR and PCA analysis. Ind. Crop. Prod. 111, 856–864.
Lehmann, J., Rillig, M.C., Thies, J., Masiello, C.A., Hockaday, W.C., Crowley, D., 2011. Biochar effects on soil biota - a review. Soil Biol. Biochem. 43, 1812–1836.
Li, H., Dong, X., da Silva, E.B., de Oliveira, L.M., Chen, Y., Ma, L.Q., 2017. Mechanisms of metal sorption by biochars: biochar characteristics and modifications. Chemosphere 178, 466–478.
Liu, Z., Zhang, F.-S., 2009. Removal of lead from water using biochars prepared from hydrothermal liquefaction of biomass. J. Hazard Mater. 167, 933–939.
Lu, H., Zhang, W., Yang, Y., Huang, X., Wang, S., Qiu, R., 2012. Relative distribution of Pb 2+ sorption mechanisms by sludge-derived biochar. Water Res. 46, 854–862.
Ma, F., Zhao, B., Diao, J., 2016. Adsorption of cadmium by biochar produced from pyrolysis of corn stalk in aqueous solution. Water Sci. Technol. 74, 1335–1345.
Mandal, A., Singh, N., Purakayastha, T.J., 2017. Characterization of pesticide sorption behaviour of slow pyrolysis biochars as low cost adsorbent for atrazine and imidacloprid removal. Sci. Total Environ. 577, 376–385.
Martucci, A., Braschi, I., Bisio, C., Sarti, E., Rodeghero, E., Bagatin, R., Pasti, L., 2015. Influence of water on the retention of methyl tertiary-butyl ether by high silica ZSM-5 and y zeolites: a multidisciplinary study on the adsorption from liquid and gas phase. RSC Adv. 5, 86997–87006.
Mašek, O., Buss, W., Sohi, S., 2018. Standard biochar materials. Environ. Sci. Technol. 52, 9543–9544.
Misono, M., Ochiai, E., Saito, Y., Yoneda, Y., 1967. A new dual parameter scale for the strength of lewis acids and bases with the evaluation of their softness. J. Inorg. Nucl. Chem. 29, 2685–2691.
Moreno, E., Beesley, L., Lepp, N., Dickinson, N., Hartley, W., Clemente, R., 2011. Field sampling of soil pore water to evaluate trace element mobility and associated environmental risk. Environ. Pollut. 159, 3078–3085.
Mukherjee, A., Zimmerman, A.R., Harris, W., 2011. Surface chemistry variations among a series of laboratory-produced biochars. Geoderma 163, 247–255.
Naidu, D.A., King, P., Saibaba, K.V.,N., Prasad, V.S.R.K., 2013. Equilibrium , kinetic and thermodynamic studies on lead removal from aqueous solution by tectona grandis L . F. Int. J. Res. Eng. Technol. 1, 35–48.
Park, J.-H., Ok, Y.S., Kim, S.-H., Cho, J.-S., Heo, J.-S., Delaune, R.D., Seo, D.-C., 2016. Competitive adsorption of heavy metals onto sesame straw biochar in aqueous solutions. Chemosphere 142, 77–83.
Park, J.H., Choppala, G., Lee, S.J., Bolan, N., Chung, J.W., Edraki, M., 2013. Comparative sorption of Pb and Cd by biochars and its implication for metal immobilization in soils. Water. Air. Soil Pollut. 224.
Pourret, O., Houben, D., 2018. Characterization of metal binding sites onto biochar using rare earth elements as a fingerprint. Heliyon 4, e00543.
Qian, T., Wang, Y., Fan, T., Fang, G., Zhou, D., 2016. A new insight into the immobilization mechanism of Zn on biochar: the role of anions dissolved from ash. Sci. Rep. 6.
R Core Team, 2013. R: A Language and Environment for Statistical Computing. R Foundation for Statistical Computing.
Ritz, C., Streibig, J.C., 2009. Nonlinear regression with R. J. Stat. Software.
Schweiker, C., Wagner, A., Peters, A., Bischoff, W.-A., Kaupenjohann, M., 2014. Biochar reduces zinc and cadmium but not copper and lead leaching on a former sewage field. J. Environ. Qual. 43, 1886–1893.
Shahbeig, H., Bagheri, N., Ghorbanian, S.A., Hallajisani, A., Poorkarimi, S., 2013. A new adsorption isotherm model of aqueous solutions on granular activated carbon. UK World J. Modell. Simulati. 9 (4), 243–254.
Shaheen, S.M., Tsadilas, C.D., Rinklebe, J., 2013. A review of the distribution coefficients of trace elements in soils: influence of sorption system, element characteristics, and soil colloidal properties. Adv. Colloid Interface Sci. 201, 43–56.
Sparks, D.L., 2003. Environmental Soil Chemistry, second ed. Ltd, Elsevier, San Diego, California.
Soria, P. Rosa Isabel, Rolfe, Stephen, Mauro, Pazmiño Betancourth, Thornton, Steven F., 2020. Dataset: the Relationship between Properties of Plant-Based Biochars and Sorption of Cd(II), Pb(II) and Zn(II) in Soil Model Systems. Mendeley Data, V1.
Su, C., Jiang, L., Zhang, W., 2014. A review on heavy metal contamination in the soil worldwide: situation, impact and remediation techniques. Environ. Skept. Critics 3, 24–38.
Sun, J., Lian, F., Liu, Z., Zhu, L., Song, Z., 2014. Biochars derived from various crop straws: characterization and Cd(II) removal potential. Ecotoxicol. Environ. Saf. 106, 226–231.
Temkin, M., Pyzhev, V., 1940. Kinetics of ammonia synthesis on promoted iron catalysts. Acta Physicochim 12, 327–356.
Trakal, L., Bingöl, D., Pohořelý, M., Hruška, M., Komárek, M., 2014. Geochemical and spectroscopic investigations of Cd and Pb sorption mechanisms on contrasting biochars: engineering implications. Bioresour. Technol. 171, 442–451.
Uchimiya, M., Wartelle, L.H., Klasson, K.T., Fortier, C.A., Lima, I.M., 2011. Influence of pyrolysis temperature on biochar property and function as a heavy metal sorbent in soil. J. Agric. Food Chem. 59, 2501–2510.
Waiapu, O., Mcmillan, T., 2018. Characteristics and Mechanisms of Atrazine Sorption to Biochar for Land Remediation.
Wang, M., Zhu, Y., Cheng, L., Andserson, B., Zhao, X., Wang, D., Ding, A., 2018. Review on utilization of biochar for metal-contaminated soil and sediment remediation. J. Environ. Sci. 63, 156–173.
Wang, Y., Wang, H.-S., Tang, C.-S., Gu, K., Shi, B., 2019. Remediation of heavy metal contaminated soils by biochar: a review. Environ. Geotech. 1–14.
Wang, Z., Liu, G., Zheng, H., Li, F., Ngo, H.H., Guo, W., Liu, C., Chen, L., Xing, B., 2015. Investigating the mechanisms of biochar's removal of lead from solution. Bioresour. Technol. 177, 308–317.
Weiss, J.N., 1997. The Hill equation revisited: uses and misuses. Faseb. J. 11, 835–841.
Wu, W., Li, Jianhong, Lan, T., Müller, K., Niazi, N.K., Chen, X., Xu, S., Zheng, L., Chu, Y., Li, Jianwu, Yuan, G., Wang, H., 2017. Unraveling sorption of lead in aqueous solutions by chemically modified biochar derived from coconut fiber: a microscopic and spectroscopic investigation. Sci. Total Environ. 576, 766–774.
Xiang, W., Zhang, X., Chen, J., Zou, W., He, F., Hu, X., Tsang, D.C.W., Ok, Y.S., Gao, B., 2020. Biochar technology in wastewater treatment: a critical review. Chemosphere 126539.

Xu, X., Cao, X., Zhao, L., Wang, H., Yu, H., Gao, B., 2013. Removal of Cu, Zn, and Cd from aqueous solutions by the dairy manure-derived biochar. Environ. Sci. Pollut. Res. 20, 358–368.

Xu, X., Zhao, Y., Sima, J., Zhao, L., Mašek, O., Cao, X., 2017. Indispensable role of biochar-inherent mineral constituents in its environmental applications: a review. Bioresour. Technol. 241, 887–899.

Yang, H., Yan, R., Chen, H., Lee, D.H., Zheng, C., 2007. Characteristics of hemicellulose, cellulose and lignin pyrolysis. Fuel 86, 1781–1788.

Yang, X., Lu, K., McGrouther, K., Che, L., Hu, G., Wang, Q., Liu, X., Shen, L., Huang, H., Ye, Z., Wang, H., 2017. Bioavailability of Cd and Zn in soils treated with biochars derived from tobacco stalk and dead pigs. J. Soils Sediments 17, 751–762.

Yang, Z., Fang, Z., Zheng, L., Cheng, W., Tsang, P.E., Fang, J., Zhao, D., 2016. Remediation of lead contaminated soil by biochar-supported nano-hydroxyapatite. Ecotoxicol. Environ. Saf. 132, 224–230.

Zhang, F., Wang, X., Yin, D., Peng, B., Tan, C., Liu, Y., Tan, X., Wu, S., 2015. Efficiency and mechanisms of Cd removal from aqueous solution by biochar derived from water hyacinth (Eichornia crassipes). J. Environ. Manag. 153, 68–73.